Fundamental Understanding of Palladium-Based Catalysts: From Pyrene-Based COFs to Size-Controlled Bimetallic Nanostructures

Hridita Purba Saha

Thesis submitted to the Faculty of the

Virginia Polytechnic Institute and State University

in partial fulfillment of the requirements for the degree of

Master of Science

in

Chemical Engineering

Ayman M. Karim, Chair

Hongliang Xin

Sheima Khatib

April 25, 2025

Blacksburg, Virginia

Keywords: Covalent Organic Framework (COF), Single-atom,

Bimetallic alloy, Selective Hydrogenation

Fundamental Understanding of Palladium-Based Catalysts: From Pyrene-Based COFs to Size-Controlled Bimetallic Nanostructures

Hridita Purba Saha

Abstract

The catalytic properties of single atoms (SAs) have attracted growing attention due to their unique electronic characteristics and their ability to maximize atomic efficiency compared to nanoparticles. As particle size decreases, the coordination environment around the metal atoms becomes increasingly unsaturated, which raises the surface free energy and enhances the reactivity of the metal species toward supports and adsorbates—this underpins the well-known size effects in metal nanocatalysts. In the extreme case of single-atom catalysts (SACs), the combination of highly active valence electrons, quantum confinement effects, and discrete energy levels leads to maximized surface free energy and distinct chemical behavior. Covalent organic frameworks (COFs), a class of porous and crystalline materials composed of light elements (H, B, C, N, and O), are attractive supports for SACs due to their designable periodic structures and stable covalent bonding. These frameworks offer uniform and tunable binding sites ideal for anchoring metal atoms. Therefore, Single metal atoms anchored on COFs offer a powerful platform for tailoring active sites, enabling the optimization of catalytic activity, selectivity, and stability, with promising potential for use in a wide range of industrial chemical processes.

Ethylene hydrogenation has long been used as a model reaction in heterogeneous catalysis to better understand the mechanism of selective acetylene hydrogenation over metal catalysts. Improving selectivity often depends on how strongly the reactants adsorb onto the metal surface. When ethylene binds more weakly to the active sites, selectivity improves—an insight that has led to growing interest in designing catalysts with isolated single metal atoms. Pd single-atom catalysts are highly valued for their activity in ethylene and acetylene hydrogenation under ambient conditions. In this work, we employed $PdCl_2$-functionalized, pyrene-based COFs that provide uniform binding sites ideal for stabilizing isolated palladium atoms. In this study, we used X-ray photoelectron spectroscopy (XPS) and diffuse reflectance infrared Fourier transform spectroscopy (DRIFTS) with CO as a probe molecule along with catalytic performance evaluation through ethylene hydrogenation kinetics.

However, the pyrene-based COF inherently incorporates palladium impurities during synthesis, and the observed catalytic activity of pristine COF can vary significantly depending on the level of these residual Pd species. This makes it difficult to distinguish between the intrinsic activity of the pristine COF and that of atomically dispersed Pd. To reduce these impurities, we implemented two monomer purification methods prior to COF synthesis: triphenylphosphine (PPh_3) treatment and acid column purification. These approaches lowered the Pd content from 0.35% to 0.23% and 0.04%, respectively. PPh_3 purification was not optimal, as it introduced structural defects in the COF, leading to higher catalytic activity compared to the non-purified COF. Conversely, acid column purification preserved the Pd and N coordination environment, revealing distinct activity differences between the 4% Pd-loaded sample and the pristine COF. Notably, even at a reduced 1% Pd loading—critical for stability under reaction conditions—a significantly higher activity than that of the pristine COF was observed. This work highlights the critical role of purification and its underlying mechanisms in shaping the coordination environment and structural integrity of COFs, which in turn significantly impacts their catalytic activity and selectivity in ethylene

and acetylene hydrogenation.

Bimetallic catalysts often outperform their monometallic counterparts and are widely used in essential chemical transformations such as selective hydrogenation, reforming, coupling, and oxidation. Among them, PdAu alloy catalysts have garnered particular interest due to their ability to undergo dynamic surface restructuring, which plays a critical role in tuning catalytic activity and selectivity. The extent of this restructuring is influenced by factors such as the Pd-to-Au ratio, nanoparticle size, and the nature of adsorbates under reaction conditions. This study investigates how surface structures in Au, Pd, and PdAu nanoparticles evolve with variations in composition, particle size, and temperature. Results show that larger and samller nanoparticles tend to form Au rich surface. Notably, increasing the temperature from cryogenic levels induces Pd migration from the core to the surface, facilitating the formation of Pd trimers. These structural changes are reversible, with Pd atoms re-segregating back into the bulk upon cooling, highlighting the temperature-sensitive and reversible nature of surface restructuring in PdAu catalysts.

Fundamental Understanding of Palladium-Based Catalysts: From Pyrene-Based COFs to Size-Controlled Bimetallic Nanostructures

Hridita Purba Saha

General Audience Abstract

Catalysts are materials that help speed up chemical reactions without being used up. One important reaction they assist with is hydrogenation, which is widely used in industrial processes such as making fuels and plastics. Ethylene, a key component in polymer production, is often made in steam crackers and usually contains about 1% acetylene as an impurity. This acetylene must be selectively hydrogenated into ethylene so it doesn't interfere with the polymerization process. Achieving this requires highly optimized and selective catalysts. In this study, we focused on a special type of catalyst made from single palladium atoms supported on a material called a covalent organic framework (COF). These single-atom catalysts are very efficient because they allow full exposure of active sites, making better use of the metal. However, during the COF synthesis, small amounts of unwanted palladium impurities can remain, which may affect the catalyst's performance. To address this, we applied two different purification methods to remove these impurities before constructing the final COF. This allowed us to gain clearer insight into the role of palladium single atoms in driving hydrogenation reactions when supported on the COF.

Acknowledgments

I would like to express my deepest gratitude to my advisor, **Prof. Ayman M. Karim**, for his continuous support, guidance, and mentorship throughout my graduate journey. His encouragement, insightful feedback, and high standards have shaped my growth as a researcher and problem-solver. I am also sincerely thankful to my committee members, **Prof. Hongliang Xin** and **Prof. Sheema Khatib**, for their guidance and support during the course of my study.

I would like to acknowledge my collaborators **Prof. Hani El-Kaderi** from Virginia Commonwealth University and **Ruby Deeter**, as well as **Prof. David Flaherty** from Georgia Tech and **Suchi Vijayaraghavan**, for their valuable scientific input and support in advancing my research. Thanks to my labmates and colleagues for their support, friendship, and collaboration: **Md Raian Yousuf**, **Hung-Ling Yu**, **Sara Haidar**, **Mohamed Mohamed Eisa**, **Vishwas Akavaram**, **Abir Poddar**, and **Yuxin Li**.

Finally, I would like to thank my parents for their unconditional love, endless encouragement, and sacrifices. I am also deeply grateful to my husband for his constant support, patience, and belief in me throughout this journey.

Contents

List of Figures

List of Tables

Chapter 1:

Optimizing Pd Single-Atom Catalysts in Pyrene-Based COFs: Purification Strategies and Catalytic Performance in Ethylene Hydrogenation

Attribution:

This project was conducted in collaboration with Professor Hani El-Kaderi and graduate student Ruby Deeter from Virginia Commonwealth University (VCU). R.D. was responsible for synthesizing the catalyst and performing XPS, XRD, and BET measurements. H.P.S. carried out the DRIFTS and kinetic experiments. Professors Ayman Karim and Hani El-Kaderi jointly conceived the research idea, planned the experimental strategy, and directed the overall project.

1.1 Introduction & Literature review

1.1.1 Single-Atom Catalyst (SAC): Role in semi-hydrogenation reaction

Hydrogenation is a fundamental process in petrochemical, coal chemical, fine chemical, and environmental industries. Among various hydrogenation transformations, selective hydrogenation stands out as a critical and highly valued reaction. Chemoselective hydrogenation occurs when multiple functional groups coexist within a single substrate, or when different unsaturated substrates are present in the catalytic system, allowing one functional group (or substrate) to undergo preferential hydrogenation while leaving others unaffected.[1] A key example is the selective hydrogenation of acetylene in an ethylene-rich environment. In this process, acetylene must be exclusively hydrogenated to ethylene, while preventing the over-hydrogenation of ethylene to ethane. This reaction is particularly crucial in the production of polymer-grade ethylene, which is obtained from steam crackers and typically contains approximately 1% acetylene as an impurity.[2, 3] To ensure efficient polymerization, the acetylene concentration must be reduced to just a few parts per million (ppm),[4, 5] as even trace amounts can negatively impact the polymerization process. Achieving this level of selectivity requires highly optimized catalysts capable of discriminating between acetylene and ethylene, ensuring that acetylene is fully converted while minimizing ethylene losses. The development of such catalysts is essential for enhancing efficiency and yield in industrial hydrogenation processes.

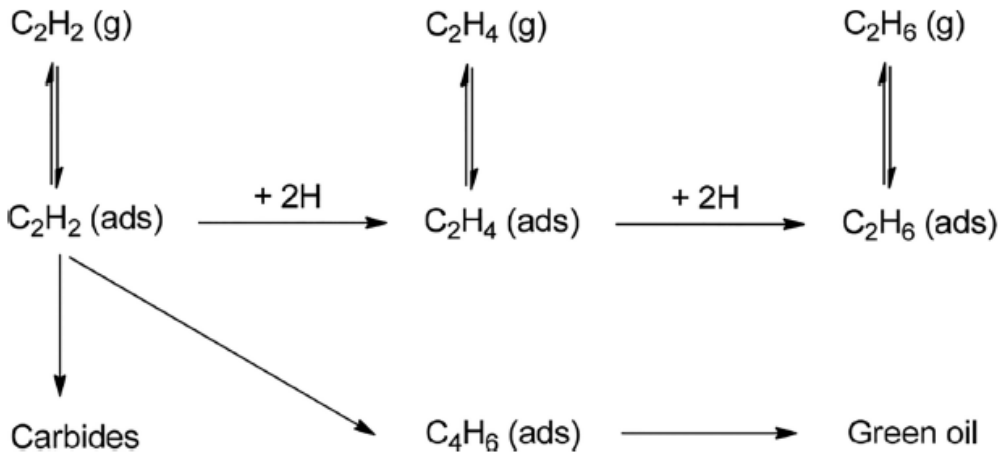

Figure 1.1: Reaction network for acetylene hydrogenation.
[1]

The efficiency of selective hydrogenation depends on the development of highly selective and stable catalysts.[6] Heterogeneous catalysts are particularly advantageous due to their ease of separation and reusability.[7, 8] The first-generation catalysts, metal complexes immobilized on oxides or resins, offer high selectivity but suffer from metal and ligand leaching. The second-generation catalysts, supported metal nanoparticles (Figure:1.1(a)),[9] improve stability but often lead to over-hydrogenation, reducing chemoselectivity. To address this, bimetallic catalysts (Sn, Pb, Bi) and organic modifiers (mercaptans, amines) have been introduced (Figure:2.1(b)),[10, 11] as seen in Lindlar catalysts (Pd/CaCO -Pb).[11, 12, 13] However, these modifications often reduce catalytic activity by blocking active sites. On this ground, a new generation of catalysts for selective hydrogenation reactions—single-atom catalysts (SACs)—was developed (Figure 1c). Owing to the ultimate dispersion of active metals and the homogeneous composition of the active species, SACs have demonstrated excellent catalytic activity and selectivity in various chemical, electrochemical, and photochemical transformations, including selective hydrogenation reactions. Moreover, they offer a valuable platform for investigating the structure–performance relationship in catalysis.

Understanding the mechanism of Pd-catalyzed semihydrogenation of trace acetylene in ethylene-rich feedstocks is crucial from both scientific and industrial standpoints, particularly for the

development and optimization of improved catalyst systems [14, 15, 16, 17]. This reaction is well known for its pronounced structure sensitivity, with catalytic performance being strongly influenced by the size of Pd particles [18, 19, 20]. Studies have shown that the Pd(111) surface facilitates acetylene conversion and the formation of C_4 byproducts, while edge sites are primarily responsible for ethane formation[21]. These observations highlight the significant role of particle size in determining both the activity and selectivity of Pd-based catalysts[19, 21].

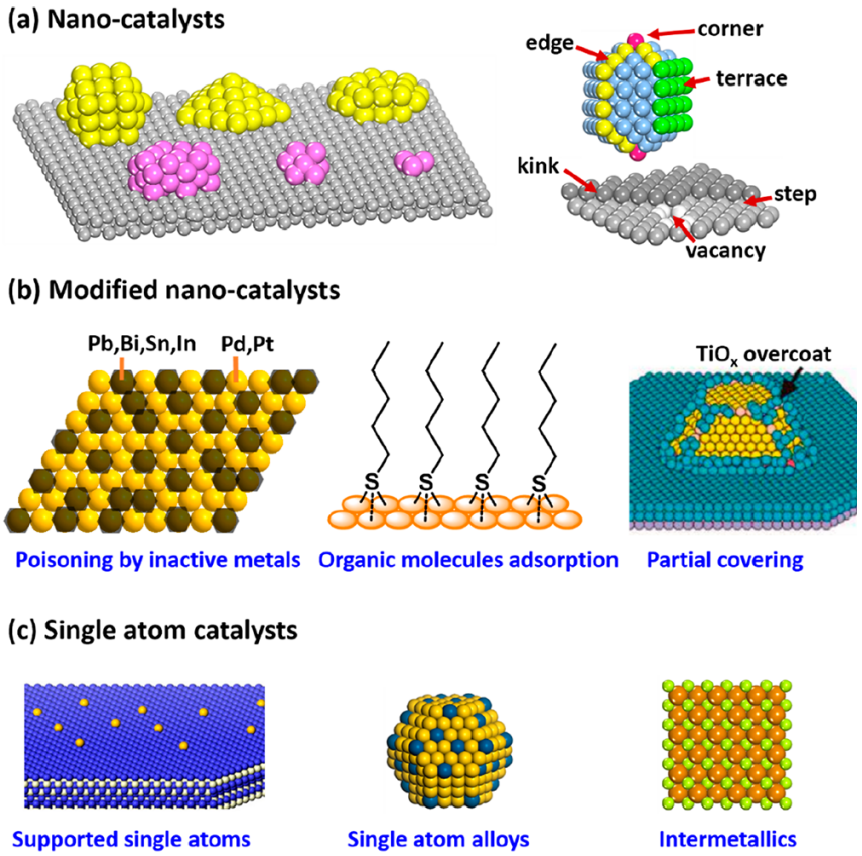

Figure 1.2: Illustration of supported nanocatalysts (a), modified nanocatalysts (b), and single-atom catalysts (c).

[1]

Beyond particle size effects, the nature of the catalyst support also plays a vital role in modulating catalytic behavior[22, 23, 24]. In many cases, changes in support material lead to simultaneous variations in Pd nanoparticle size and electronic properties. When reducible or

acidic metal oxides are employed as supports, metal-support interactions and the acidity of the support can influence catalyst stability and coke formation. To mitigate these complications, chemically inert and weakly interactive supports such as α-Al_2O_3 are commonly used in commercial applications[25, 26]. Alternative supports like carbon materials have demonstrated beneficial effects on catalyst performance. The weak acidity of carbon has shown minimal influence on deactivation[27], while the use of carbon-supported Pd catalysts has led to improved activity in acetylene semihydrogenation compared to their alumina-supported counterparts[28]. Additionally, carbon offers several advantageous characteristics, including high surface area for metal dispersion, tunable surface chemistry, and efficient electron transfer at the metal–support interface. These unique properties underscore the importance of further investigating the structural and kinetic aspects of support effects to guide rational catalyst design.

One prerequisite for designing chemoselective catalysts is a clear understanding of the reaction mechanism that governs selectivity. It is widely accepted that chemoselectivity is largely determined by the adsorption strength and configuration of reactants or intermediates on the catalyst surface, which, in turn, is influenced by the electronic and geometric structures of the active sites.[29, 30] For instance, on a Pd surface, ethylene can adopt three distinct adsorption modes depending on the local Pd atomic configuration: ethylidyne mode on three-fold sites, di-σ mode on two-fold sites, and π-bonded mode on isolated Pd single atoms. The adsorption strength follows the trend: ethylidyne $>$ di-σ $>$ π-bonded.[29, 31] In the semihydrogenation of acetylene, the weakest adsorption mode (π-bonded) facilitates ethylene desorption, preventing further hydrogenation to ethane.

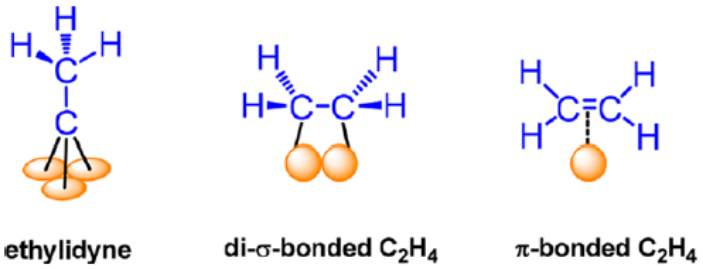

Figure 1.3: Adsorption patterns of ethylene on Pd catalysts with different geometric structures.

[1]

Similarly, when two or multiple functional groups coexist in the substrate and each of them can be adsorbed on the catalyst, there will be multiple adsorption patterns and consequently various products and poor chemoselectivity. Therefore, to achieve excellent chemoselectivity, it is highly desirable to allow only the target functional group to be adsorbed on the catalyst in a proper pattern. Consequently, isolation of Pd as single atoms is essential for achieving high ethylene selectivity. This requires catalytic active sites with uniform geometric and electronic structures, minimizing unwanted adsorption patterns and ensuring selective transformation.

1.1.2 Covalent Organic Framework (COF)

Nanoporous materials have garnered significant attention due to their exceptional properties and diverse applications across multiple disciplines, including physics, chemistry, and biology.[32, 33, 34, 35, 36, 37], Recently, covalent organic frameworks (COFs) have emerged as a novel class of covalent crystalline polymers characterized by high porosity and low crystal density. Since their first successful synthesis by Yaghi and colleagues in 2005, COFs have generated considerable interest in the field of porous materials. The pioneering structures, COF-1 $[C_3H_2BO)_6 \cdot (C_9H_{12})_1]$ and COF-5 $[C_9H_4BO_2]$, were synthesized via a straightforward one-pot reaction.[38]

COFs can be broadly categorized into two-dimensional (2D) and three-dimensional (3D)

frameworks, depending on the geometries of their building blocks. In 2D COFs, covalently bonded frameworks assemble into atomic layers that stack through π–π interactions, forming ordered layered structures. The presence of template-directed polymerization in their synthesis facilitates their formation, while their extended π-conjugated skeletons provide a robust platform for structural modifications. Conversely, 3D COFs are composed of covalently interconnected building units that create extended three-dimensional networks. These materials exhibit ultra-low densities (as low as 0.17 g/cm^3)[39], large surface areas, and numerous open sites, making them highly suitable for applications such as gas storage, separation, catalysis, and optoelectronics.[40, 41, 42] Based on the structural characteristics of their building blocks, covalent organic frameworks (COFs) synthesized to date can be broadly classified into three main categories: boron-containing COFs, nitrogen-containing COFs, and silicon-containing COFs.[43] Notably, compared to boron- and silicon-based COFs, the recently developed nitrogen-containing COFs, constructed through C–N bond formation, exhibit superior chemical stability, making them well-suited for catalytic applications. Among these, imine-linked COFs, which feature C=N bonds with polarized electron distribution—resulting in partially positive carbon and partially negative nitrogen—demonstrate high crystallinity and remarkable resistance to water, acidic, and basic conditions [39].

COFs have also demonstrated significant promise in catalysis. Their well-defined porous channels and tunable pore sizes allow efficient access to active sites and facilitate rapid mass transport during catalytic reactions.[44] The large surface areas of COFs enable the dispersion of catalytic sites, thereby enhancing reaction efficiency and selectivity. Furthermore, their polymeric frameworks, composed of modular organic building blocks linked via strong covalent bonds, exhibit remarkable thermal and chemical stability. The periodic and ordered arrangement of these frameworks, achieved with atomic precision, provides an ideal platform for the rational design of functional catalysts. By incorporating diverse catalytic sites, such as metal centers or chiral molecules, COFs can be tailored to enhance catalytic activity and significantly improve turnover numbers, making them highly versatile materials for advanced

catalytic applications. Wang et al. first demonstrated the catalytic application of COFs in 2011 by preparing Pd/COF-LZU1 via post-metalation of a 2D imine-linked COF and testing it in the Suzuki-Miyaura coupling reaction.[45] After that, several examples highlight the promising catalytic performance of metal-functionalized COFs. For instance, Pd/COF-LZU1 containing singly dispersed palladium acetate has demonstrated excellent activity in cross-coupling reactions [45, 46, 47]. Similarly, COF-367-Co with isolated cobalt atoms embedded in an extended COF framework has shown remarkable efficiency and selectivity for electrocatalytic CO_2 reduction to CO [48]. Additionally, tuning the spin state of cobalt within this framework can significantly influence its photocatalytic behavior [49]. Other metal-coordinated COFs, such as Co-TpBpy, Ni-TpBpy, and Cu-TpBpy, utilize bipyridine units as anchoring sites and have been developed for robust water oxidation, CO_2 photoreduction, and cycloaddition reactions, respectively [50, 51, 52]. Triazine-based building units, commonly used in the design of two-dimensional COFs, are also widely employed for catalysis as well as gas adsorption and separation applications [53, 54]. Recent studies have shown that - interactions between COF linkers and metal nanoparticles can enhance catalytic activity, exhibiting up to tenfold higher performance in selective hydrogenation reactions.[55]

1.2 Objective of this project

In this work, we utilized $PdCl_2$-functionalized, pyrene-based COFs, which offer uniform binding sites crucial for immobilizing metal single atoms. The simple Py-1P ILCOF was chosen for this study due to the high crystallinity and rigid structure of the 1,3,6,8-tetrakis(4-aminophenyl)pyrene (PyTTA) monomer, where the only heteroatoms present in the system are the imine nitrogen atoms linking the COF structure together. It was observed during the synthesis of the PyTTA monomer that a palladium catalyst is used in the Suzuki cross-coupling reaction, introducing palladium contamination into the monomer. Cross-coupling reactions are common methods for synthesizing aldehyde and amine derivatives of pyrene, and they are most efficient when a palladium catalyst is employed. An alternative

route to synthesize pyrene-amine derivatives involves reducing nitro groups to amines. However, reduction using Pd/C and a hydrogen source is the most effective and safest method. Therefore, both synthetic pathways for functionalized pyrene derivatives allow for palladium contamination, which can interfere with and impact the catalytic activity of COF supports. No study has been reported on the role of Pd impurities in pristine COFs, complicating the distinction between the activity of Pd single atoms and the pristine COF itself. To reduce these impurities prior to COF synthesis, we applied PPh_3 treatment and acid column purification, significantly lowering Pd impurities in the pristine monomer. The PPh_3 and acid treatments reduced the Pd content in the COF from 0.35% to 0.23% and 0.04%, respectively. The $PdCl_2$@Py-1P COF catalyst was characterized using various spectroscopic techniques, including X-ray photoelectron spectroscopy (XPS) and Fourier transform infrared spectroscopy (FTIR) of adsorbed CO, and its catalytic performance was evaluated for ethylene hydrogenation. This study highlights the critical role of monomer purification in optimizing the activity of Pd single atoms within the COF structure and demonstrates the impact of purification processes on COF properties and catalytic performance.

1.3 Experimental Procedures

1.3.1 Catalyst Preparation

All starting materials were used without further purification unless otherwise specified. 1,3,6,8-tetrabromopyrene (95%), 4-aminophenylboronic acid pinacol ester (98%) and tetrakis(triphenylphosphine)palladium(0) (98%) were purchased from AmBeed. Potassium carbonate (99%), terephthalaldehyde (98%), and triphenylphosphine (99+%) were purchased from Alfa Aesar. 1,2-dichlorobenzene (99%), bis(benzonitrile)palladium(II) dichloride (99+%), and Celite® 545 were purchased from Acros Chemicals. 1,4-dioxane (99+%) was purchased from Thermo Scientific. Toluene (Certified ACS, 99.9%) and hydrochloric acid (Certified ACS Plus, 36.5–38.0% w/w) were purchased from Fisher Scientific. Finally,

n-butanol (99.9%) and anhydrous chloroform (≥99%) were purchased from Sigma Aldrich.

The PYREX tubes used were of inner diameter 9.7mm, outer diameter 12mm, and length 26.5cm. 1,3,6,8-tetrakis(4-aminophenyl)pyrene and Py-1P COF were synthesized according to modified literature methods.

1.3.1.1 PyTTA Monomer Synthesis

To synthesize Py-1P COF, the 1,3,6,8-tetrakis(4-aminophenyl)pyrene (PyTTA) monomer must first be prepared via a Suzuki-Miyaura cross-coupling reaction. This process begins by combining 1,3,6,8-tetrabromopyrene (1 g, 1.94 mmol), 4-(4,5-dimethyl-1,3,2-dioxaborolan-2-yl)aniline (2 g, 9.10 mmol), and potassium carbonate (1.44 g, 10.4 mmol) in a solution of 1,4-dioxane and water (80 mL:16 mL). The system is purged by bubbling nitrogen gas for at least 30 minutes while the catalyst system is prepared. In an argon-filled glovebox, tetrakis(triphenylphosphine)palladium(0) (0.2 g, 0.18 mmol) is dissolved in 1,4-dioxane (10 mL) and stirred for 10 minutes. The catalyst solution is then transferred via cannula to the reaction system, which is fitted with a condenser and maintained under continuous nitrogen flow at 105 °C for 72 hours.

After completion, the reaction mixture is cooled to room temperature and filtered through celite. Water is added to the filtrate to induce precipitation of the monomer, followed by a second filtration to collect the solid product. The monomer is then dried under vacuum at 80 °C. This synthesis introduces palladium contamination of 0.46 weight percent from the catalyst, necessitating further purification.

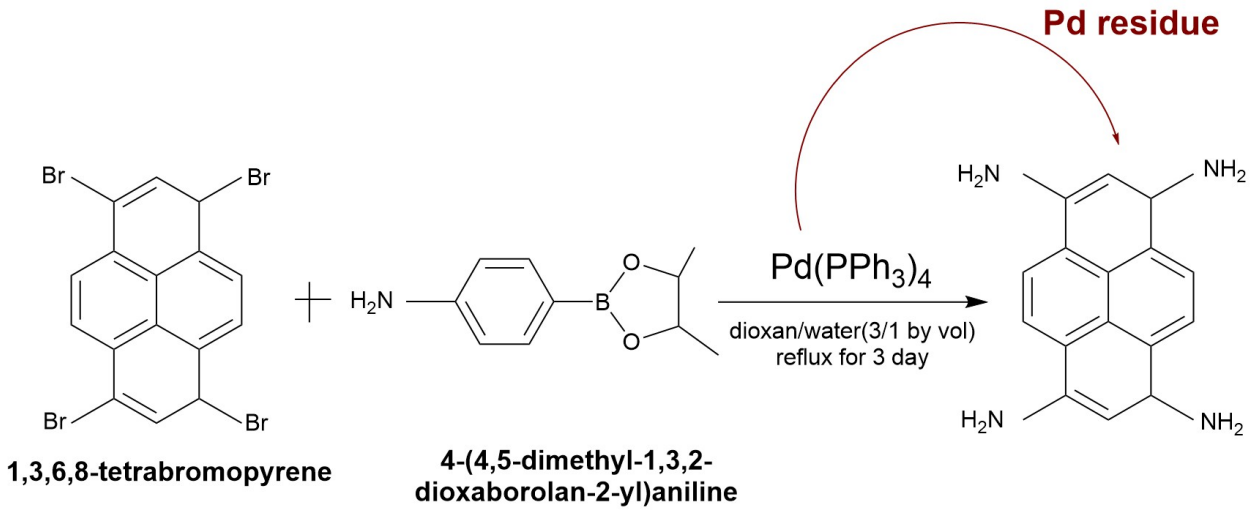

Figure 1.4: PyTTA monomer synthesis

1.3.1.2 PyTTA Monomer Purification

Triphenylphosphine Method:

The PyTTA monomer (613.1mg) was suspended in 100mL toluene in a Schlenk flask while being purged with nitrogen for 30 minutes. Triphenylphosphine (601.4mg) was massed and added to the flask. The system was then flushed with nitrogen before being sealed and allowed to stir at room temperature for 12 hours. The solution was then filtered and the monomer dried under vacuum at 80. This method reduced the palladium contamination to 0.36 wt.% by ICP (472.0mg, 77% yield).

Acid column method:

To find a method to remove the palladium contamination, the synthesized monomer (500mg) was placed in a beaker with 125mL of deionized water. Hydrochloric acid (2 M) was dropped into the water in a minimal amount until the monomer dissolved (5.5mL acid). The monomer was sonicated, as needed, to disperse larger chunks while dissolving. The solution was then placed into a column (16.5 cm L, 28.1 mm D) filled with 5 inches of celite and allowed to pass through. After collecting the filtrate, the monomer was precipitated with 0.25 M sodium hydroxide until the pH tested to 14 via indicator paper (~ 50mL). The monomer was then filtered through a medium porosity glass frit and freeze dried. This method reduced the

palladium contamination to 0.05 wt.% based on ICP (447.1mg, 89% yield).

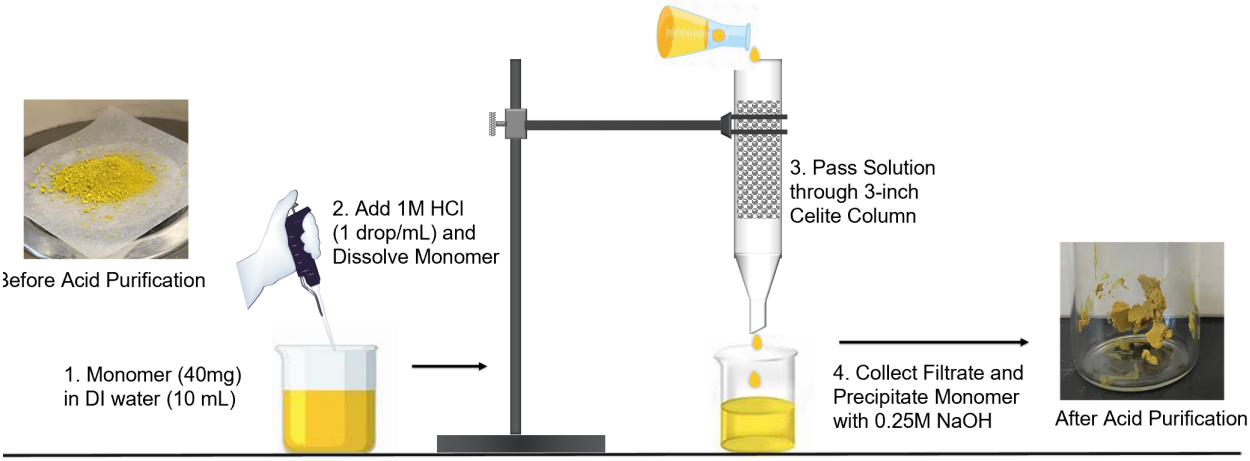

Figure 1.5: Acid purification method

1.3.1.3 Py-1P COF Synthesis

The Py-1P COF was synthesized via a solvothermal PYREX tube method, as illustrated in Figure: 1.5. Each PYREX tube was charged with 45.2 mg of the dried, synthesized PyTTA monomer and 21.5 mg of terephthalaldehyde. Then, 2 mL of *n*-butanol and 2 mL of *o*-dichlorobenzene were added and the mixture was sonicated for 10 minutes to create a uniform suspension. After the suspension was achieved, 0.4 mL of acetic acid (6 M) was added, and the tube was flash frozen in liquid nitrogen. This marked the beginning of the first of three freeze-pump-thaw cycles to degas the system. Following the third cycle, the tube was flame-sealed and placed in an oven at 120 °C for 72 hours.

Upon completion of the reaction, the tubes were broken, and the contents were filtered and washed with acetone until the filtrate ran clear. The material was then placed in a Soxhlet extractor with tetrahydrofuran (THF) for 24 hours. Finally, the product was dried under vacuum at 80 °C for 12 hours to yield a golden powder.

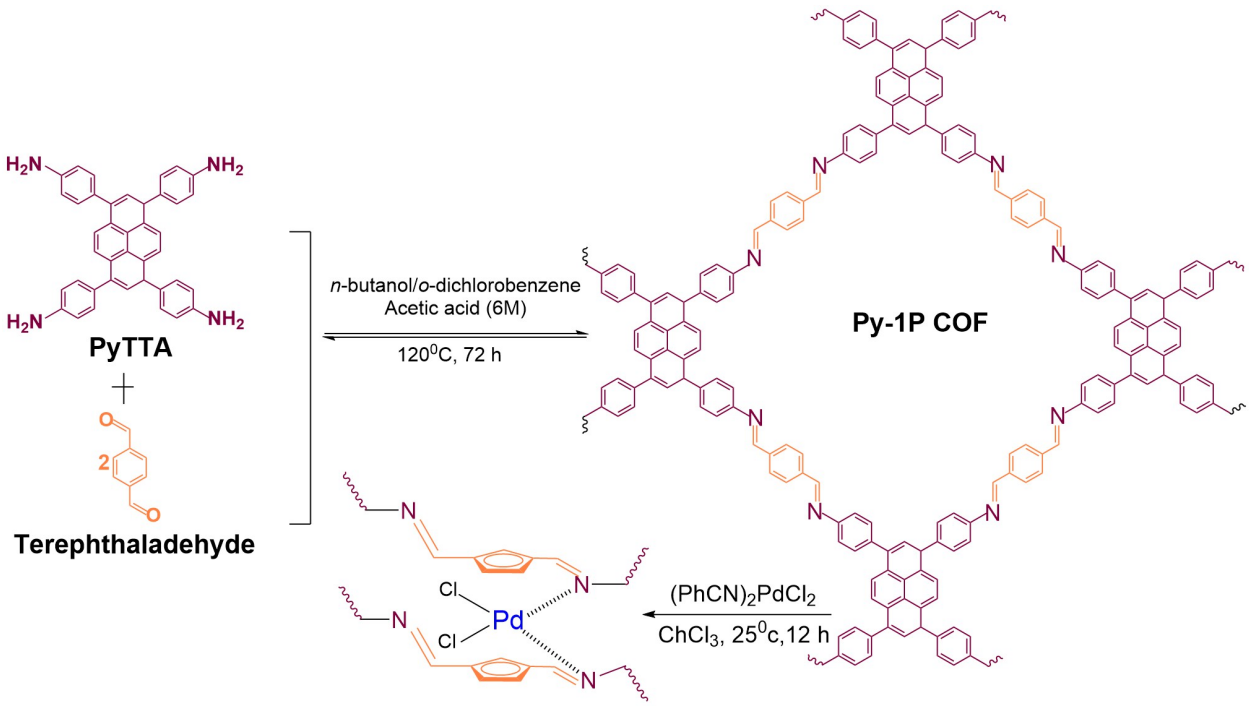

Figure 1.6: Py-1P COF synthesis

1.3.1.4 Pd@Py-COF Synthesis

The preparation of Pd@Py-1P COF is shown in Figure: 1.5 and was performed in an inert argon-filled glovebox. Anhydrous chloroform (20 mL) was used to suspend 150 mg of the COF in a Schlenk flask. A solution of bis(benzonitrile)palladium(II)chloride in anhydrous chloroform (5.5 mg: 18 mL) was made according to the targeted weight loading. The palladium solution was then added to the COF suspension dropwise to guarantee even dispersion of the single atoms. The solution was then filtered and washed in a chloroform Soxhlet extractor for 12 hours. The sample was dried under vacuum.

1.3.2 Catalyst Characterization

Surface area analyses and pore size distributions were collected on a Micromeritics 3Flex with a Smart VacPrep degassing chamber. All samples were degassed at 90 °C for 300 minutes and 120 °C for 600 minutes before undergoing analysis. Powder X-ray diffraction spectra

were collected on a Panalytical X'Pert Pro multipurpose diffractometer (Cu Kα radiation). Samples were mounted on a zero-background sample holder and measured with a 2θ range of 0–70°. A Thermo Scientific ESCALAB 250 microprobe was used to collect the XPS spectra. ICP-OES data was collected on an Agilent Technologies 5110 ICP-OES equipped with an SPS 4 autosampler.

DRIFTS of CO adsorption was conducted using a Thermo Fisher Scientific Nicolet iS50 FTIR spectrometer equipped with a liquid nitrogen-cooled mercury-cadmium-telluride (MCT) infrared detector. The catalyst was loaded into the sample cup of an *in situ* Praying Mantis diffuse reflection cell (Harrick Scientific Products). Prior to CO chemisorption, the catalyst was dried under a 100 sccm N_2 flow at 120 °C for 2 hours. Following the N_2 treatment, the sample was cooled to –120 °C using liquid nitrogen under a continuous N_2 flow. A background spectrum was collected at –120 °C under N_2 and subtracted from all subsequent spectra.

The catalytic performance of the $PdCl_2$@Py-1P COF catalyst and its respective pristine COF was evaluated for ethylene hydrogenation in a quartz packed-bed reactor under differential conditions:

$$C_2H_4 + H_2 -> C_2H_6 \quad \left(\Delta H^\circ = -137\,\frac{\text{kJ}}{\text{mol}}\right)$$

To minimize transport limitations, the 4.0 wt% $PdCl_2$@Py-1P COF catalyst was diluted intrapellet with silica gel (SiO_2, 0.075–0.250 mm, 150 Å, ACROS Organics), which was calcined in air at 800 °C prior to use. The catalyst-SiO_2 mixture was prepared to achieve a final Pd loading of 0.08 wt%. The materials were ground using an agate mortar and pestle, pelletized, and sieved to obtain 180–300 µm pellets. A total of 0.075 g of the diluted catalyst mixture was loaded into a 0.75-inch OD glass packed-bed reactor. Before catalytic testing, the catalyst was dried at 120 °C under a 100 sccm He flow for 2 hours and subsequently

cooled to 22 °C.

All catalytic activity measurements were conducted at atmospheric pressure. The gas composition of the reactor effluent was analyzed using an online gas chromatograph (MicroGC Fusion Gas Analyzer, Inficon). Ethylene (C_2H_4) and ethane (C_2H_6) were separated using an Rt-Alumina Na_2SO_4 packed column and quantified with a thermal conductivity detector (TCD). High-purity feed gases—H_2 (UHP, 99.999%), 20% C_2H_4 (certified gas, Airgas), and He (UHP, 99.999%)—were obtained from Airgas. H_2 and He were further purified using high-capacity moisture and oxygen traps (Restek catalog #20600). All gas flows were regulated by mass flow controllers (5850EM, Brooks Instrument).

Ethylene conversion and reaction rate were assessed based on the rate of reaction per gram of COF per second to distinctly compare the catalytic activity of the pristine COF and the Pd-loaded sample. This normalization to the total COF mass enables a direct evaluation of catalytic performance, providing insight into the contribution of Pd impurities in the pristine COF to its inherent activity.

$$\text{Conversion} = \frac{\text{mol of } C_2H_6 \text{ (outlet)}}{\text{mol of } C_2H_4 \text{ (inlet)}} \tag{1.1}$$

$$\text{Reaction Rate} = \frac{C_2H_6 \text{ formation rate (mol s}^{-1}\text{)}}{\text{Weight of COF (before dilution, mg)}} \tag{1.2}$$

The hydrogenation reaction was performed at 22 °C with a partial pressure of C_2H_4 at 5 kPa and H_2 at 5 kPa. Ethane was the sole detected product, and no measurable conversion of C_2H_4 or H_2 was observed in the absence of the catalyst.

1.4 Results & Discussion

The effect of monomer purification on the final palladium (Pd) content and structural quality of the synthesized Py-1P COFs was systematically investigated. Table 1.1 summarizes the Pd content of pristine and Pd-loaded COFs, as well as the Pd levels in purified and unpurified monomers and the associated percent removal. Among the purification methods tested, acid column purification was the most effective, reducing the Pd content in the monomer from 0.46 wt% to 0.05 wt%, corresponding to an 89% removal efficiency. In contrast, PPh_3 purification achieved only a 22% removal. The acid purification method is believed to remove palladium impurities by dissolving the monomer, while the insoluble palladium species are retained on the Celite stationary phase during column filtration. In contrast, the PPh_3 purification method is believed to improve the solubility of Pd contaminants by facilitating coordination between PPh_3 and Pd species present on the suspended PyTTA monomer. However, this approach may be less effective at removing palladium if the resulting $Pd(PPh_3)$ complexes are not efficiently separated from the monomer during the filtration process. The $PdCl_2$@Py-1P COF catalyst was characterized using various spectroscopic techniques, including X-ray photoelectron spectroscopy (XPS) and Fourier transform infrared spectroscopy (FTIR) of adsorbed CO, and its catalytic performance was evaluated for ethylene hydrogenation.

Table 1.1: Pd content and purification efficiency for Py-1P COFs under different monomer purification methods.

Purification Method	**Sample**	**Sample Pd Content (wt%)**	**Purified Monomer Pd Content (wt%)**	**Initial Monomer Pd Content (wt%)**	**Percent Removal**
Acid Column	Pristine Pd Loaded	0.04 4.92	0.05	0.46	89
PPh_3	Pristine Pd Loaded	0.23 3.40	0.36	0.46	22
Unpurified	Pristine Pd Loaded	0.35 4.19	0.45	N/A	N/A

1.4.1 Physical Properties of Py-COF & 4%Pd@Py-COF

Analysis was performed before and after the samples were loaded with palladium, and a post-loading decrease in surface area was observed consistently across all samples. However, the extent of the decrease varies depending on the purification method. For the unpurified COF sample, the pristine surface area was 2294 m^2/g, which dropped to 1813 m^2/g after palladium loading (Figure 1.7 (A)). This corresponds to a 21% decrease. The effect is less pronounced when the PyTTA monomer is purified prior to COF synthesis. In the sample purified with PPh_3, the surface area decreased by 12%, from 1887 m^2/g to 1666 m^2/g (Figure 1.7(B)). The acid column purification method resulted in the smallest reduction, with a 6% decrease from 1936 m^2/g to 1812 m^2/g (Figure 1.7(C)). These results indicate that purification of the PyTTA monomer is important for preserving surface area in the final COF structure. Pore size distribution was calculated according to nonlocal density functional theory (NLDFT; N_2@77 K – Carb Cyl Pores, SWNT) and was found to be consistent across pristine and Pd-loaded samples. The pore size distributions exhibit a pore width of approximately 2.3 nm, confirming the mesoporosity of the COF samples.

Table 1.2: Surface Area, Pore Size for Pristine and Pd-Loaded Py-1P COFs

Purification Method	**Sample**	**Surface Area (m^2/g)**	**Percent Decrease**	**Pore Size (nm)**
Unpurified	Pristine	2294	21	2.3
	4% Pd Loaded	1813		2.3
Acid Purified	Pristine	1936	6	2.3
	4% Pd Loaded	1812		2.3
PPh_3 Purified	Pristine	1887	12	2.3
	4% Pd Loaded	1666		2.3

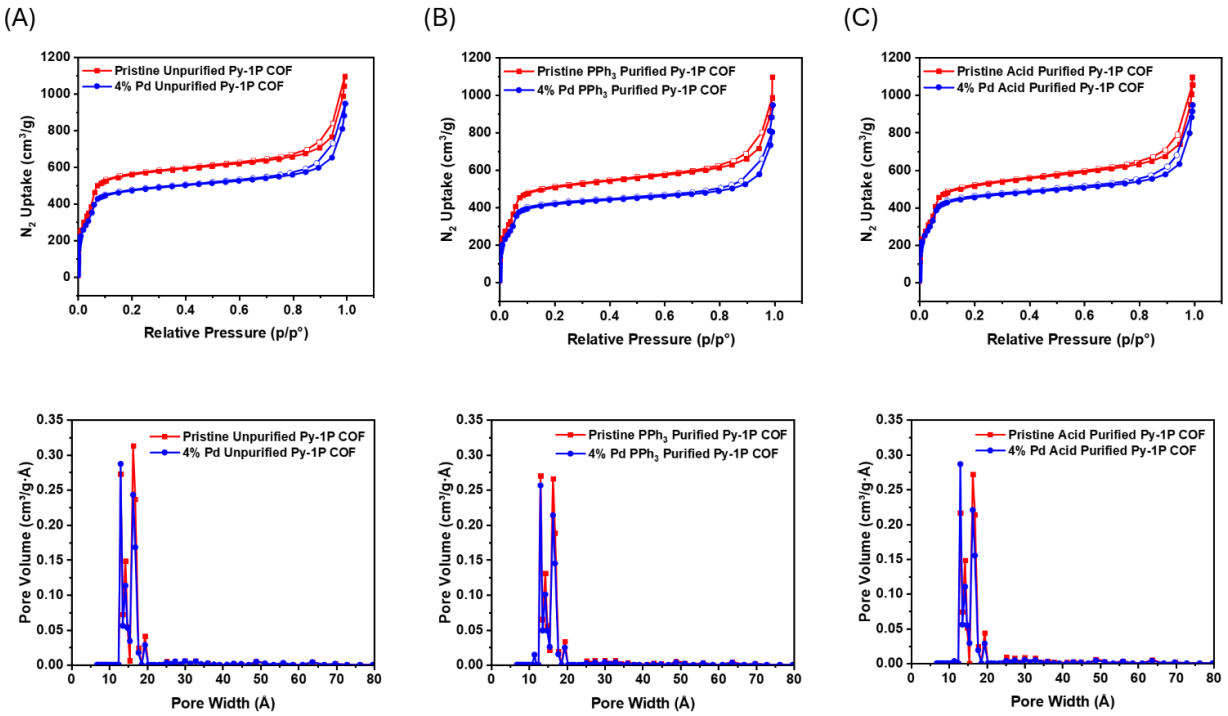

Figure 1.7: Physical properties of the Py-COF and $PdCl_2$@Py-COF catalyst: (a) Unpurified Pristine COF; (b) PPh_3-Purified Pristine COF; (c) Acid-Purified Pristine COF. Pristine Pyrene COF (Red); 4% Pd@Py-COF (Blue).

All powder X-ray diffraction (PXRD) patterns were collected using a Panalytical X'Pert Pro multipurpose diffractometer with Cu Kα radiation. All samples exhibit the characteristic diffraction peaks of Py-1P COF, corresponding to the (110), (200), (220), (310), (330), (420), (440), and (001) planes.[56] Notably, the Pd-loaded samples display enhanced crystallinity compared to their pristine counterparts, as evidenced by the increased intensity of all peaks—most prominently the (001) reflection at $2\theta = 24°$, which corresponds to the stacking of COF layers along the z-axis. This enhancement suggests potential coordination of Pd single atoms between COF layers via imine nitrogen atoms.

This peak varies in intensity across samples and is most pronounced in the non-purified pristine COF. The XRD patterns also indicate the presence of Pd clusters in the pristine COF, which are significantly reduced in intensity after purification, suggesting effective removal of Pd impurities. Maintaining high crystallinity and similar pore size are both very important

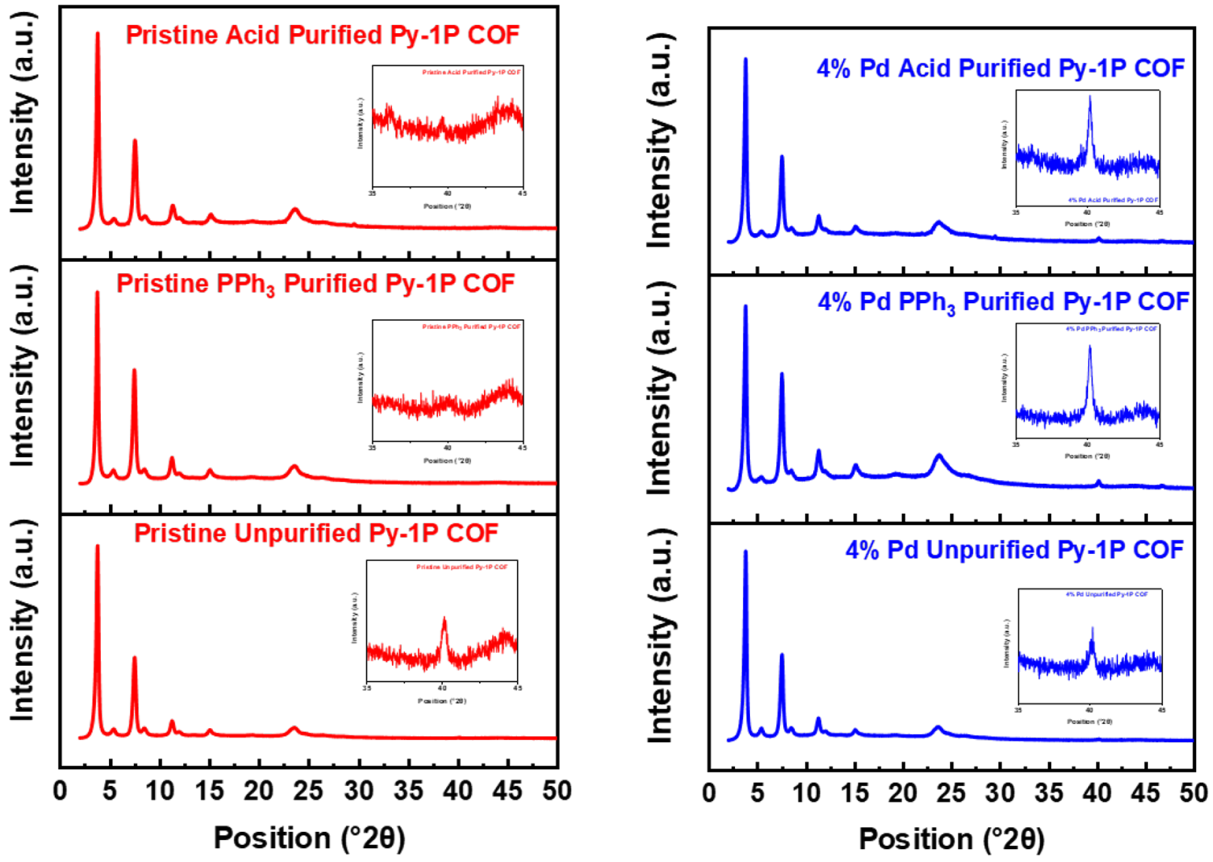

Figure 1.8: Powder X-ray Diffraction Studies of (a) Pristine COFs (Red) (b) 4% Pd@Py-COF (Blue)

in terms of catalytic applications in order to maintain full accessibility to the palladium catalytic centers aligned along the channels of the framework and to allow rapid mass transport of reactants and products.

1.4.2 Local co-ordination and local properties of Pd

X-ray photoelectron spectroscopy (XPS) is a powerful surface-sensitive technique used to analyze the elemental composition and chemical states of materials. In this study, XPS was employed to investigate the presence and chemical nature of Pd contamination in the pristine Py-1P COF.

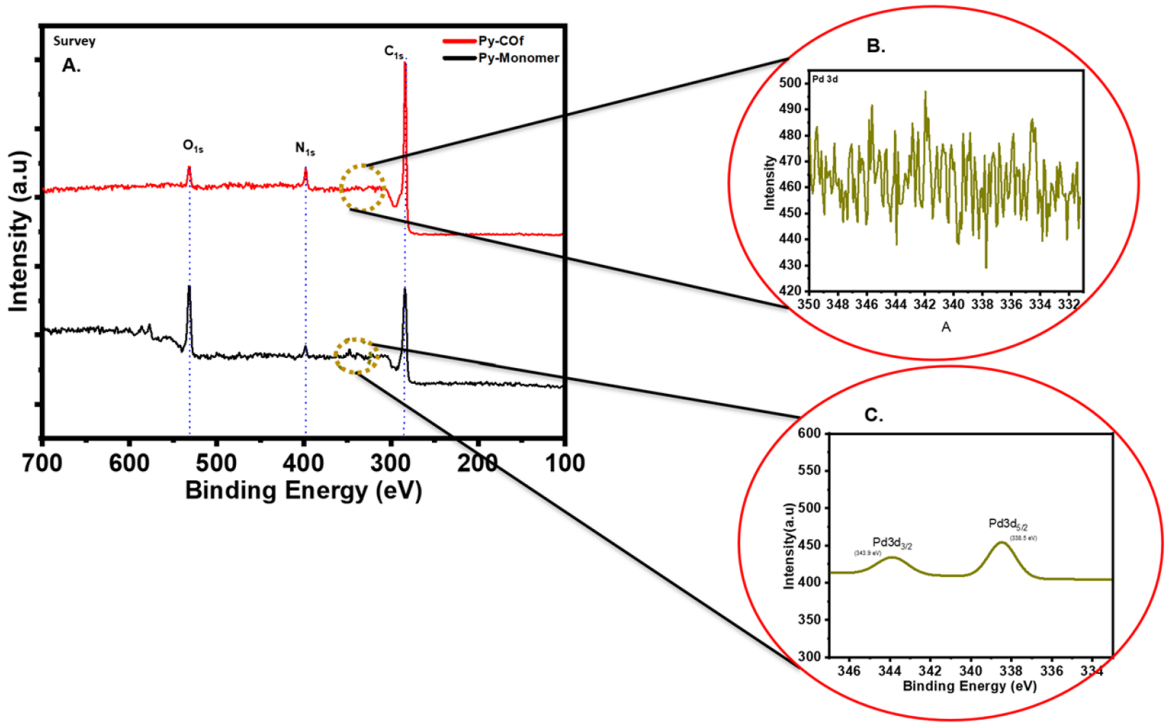

Figure 1.9: XPS results for Py-1P COF and its commercially available monomer for palladium from the survey scans

Figure 1.9 shows the survey scans of the Py-1P COF and the commercial PyTTA monomer. Both spectra exhibit no distinct palladium peaks, indicating that Pd is present only in trace amounts. Figure 1.9(B) and Figure 1.9(C) present the high-resolution scans in the Pd 3d region for the COF and the monomer, respectively. The spectrum of the COF (Figure 1.9 (B)) displays a high noise level with no resolvable Pd peaks, suggesting that the Pd concentration is below the detection limit relative to the dominant carbon and nitrogen signals.

In contrast, the monomer spectrum (Figure 1.9(C)) reveals low-intensity peaks at binding energies of 338.5 eV and 343.9 eV, corresponding to the Pd $3d_{5/2}$ and Pd $3d_{3/2}$ orbitals. These binding energies indicate that Pd is present in a coordinated form rather than as PdO or metallic Pd. This confirms that palladium is introduced during monomer synthesis and is present in a chemically bound state.

The high-resolution N_{1s} XPS spectra for the pristine Py-1P COF samples (Figure 1.10) show a consistent peak at approximately 399.2 eV across all purification conditions—acid

purified, PPh_3 purified, and unpurified—indicating that the nitrogen environment in the imine linkage remains structurally similar regardless of the monomer purification method. This peak corresponds to the nitrogen in the C=N imine bond, which is the dominant nitrogen species in the COF framework. The palladium-loaded sample exhibits a single nitrogen peak, which appears broadened due to the presence of two distinct binding environments: one corresponding to uncoordinated imine nitrogen (399 eV) and the other to imine nitrogen coordinated to palladium (400 eV). This shift confirms the successful coordination of Pd(II) species to the nitrogen atoms of the COF. Interestingly, among the Pd loaded samples, the PPh_3-purified COF shows a noticeably broader N_{1s} peak compared to the acid-purified and unpurified samples. This broadening may be attributed to a more heterogeneous nitrogen environment, possibly arising from defect sites or varying local bonding environments introduced during the purification process. These subtle spectral differences offer further insight into how monomer purification impacts the structural uniformity of the resulting COFs and their capacity to host atomically dispersed metal sites.

Figure1.11 shows the Pd 3d XPS spectra of 4% Pd-loaded Py-1P COF under three different purification conditions: unpurified, PPh_3 purified, and acid purified. Each spectrum features two distinct Pd spin-orbit doublets, corresponding to palladium in different chemical environments—PdO and PdN. The PdO signals appear at lower binding energies, with Pd $3d_{5/2}$ and Pd $3d_{3/2}$ peaks around 336.5–337.1 eV and 341.8–342.1 eV, respectively. In contrast, the PdN signals are shifted to higher binding energies, near 338.2–338.4 eV and 343.4–343.5 eV.

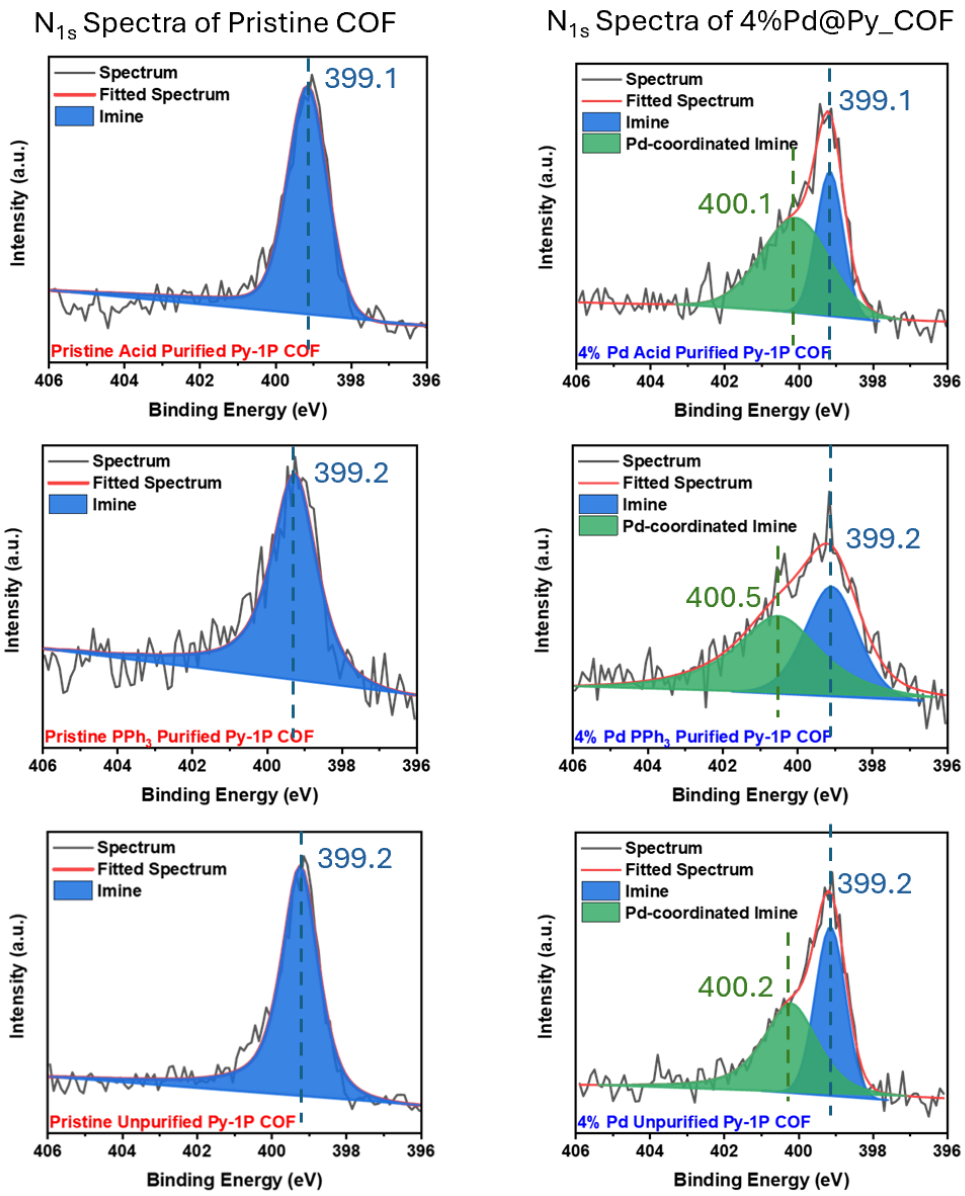

Figure 1.10: XPS results for Py-1P COF and its commercially available monomer for palladium from the survey scans

In both the unpurified and acid purified samples, the PdN peaks are more intense, suggesting a greater extent of palladium coordination with nitrogen within the COF framework. Conversely, the PPh_3 purified sample exhibits a diminished PdN signal, indicating a lower degree of Pd–N interaction. These results demonstrate that the purification method significantly influences the local chemical environment of palladium, which may in turn affect the catalyst's performance.

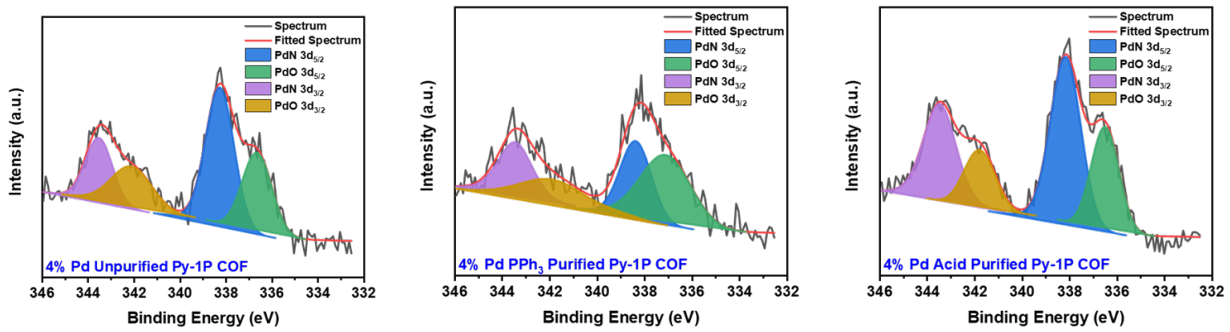

(a) (b) (c)

Figure 1.11: Comparison of Pd_{3d} XPS spectra for (a) 4% Pd Unpurified Py-COF (b)4% Pd PPh_3 purified Py-COF (c) 4% Pd Acid Py-COF

To evaluate the homogeneity of the local coordination environment of Pd atoms in the $PdCl_2$@Py-1P COF catalyst, CO adsorption experiments were conducted at –120°C using diffuse-reflectance infrared Fourier transform spectroscopy (DRIFTS). A symmetric and relatively narrow band was observed at 2,129 cm^{-1}, with a full width at half maximum (FWHM) of approximately 20 cm^{-1} Figure:1.12. No additional CO adsorption bands were detected in the 1,800–2,200 cm^{-1} region, where vibrational modes associated with linear, bridge, and hollow site adsorption on Pd typically appear. This absence indicates that Pd is present predominantly as isolated single atoms. Moreover, the consistent peak position and bandwidth across samples prepared with different monomer purification protocols suggest that these treatments have minimal influence on the post-synthetic modification strategy used to achieve a 4 wt% Pd single-atom loading. A minor shoulder at higher wavenumbers is attributed to the presence of small oxidized Pd species, likely introduced during the filtration

process conducted under ambient conditions.

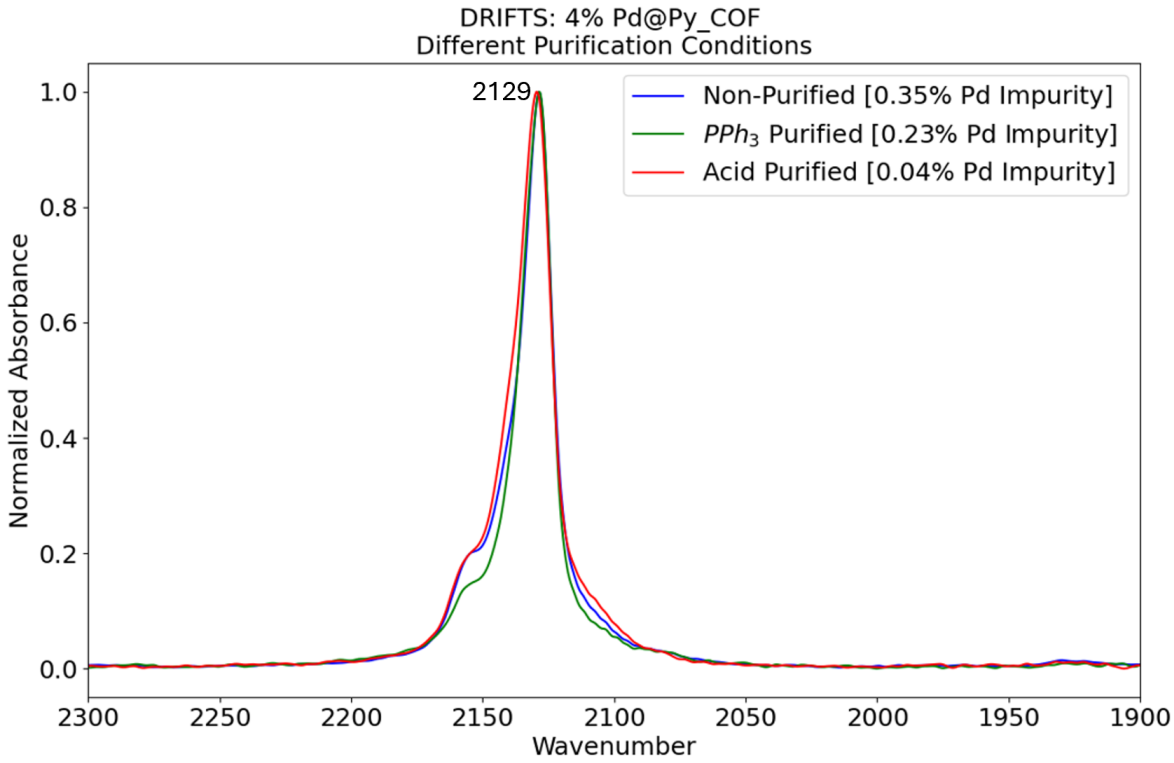

Figure 1.12: DRIFTS spectra of CO adsorption on the 4% Pd@Py-COF catalyst for different purification process

1.4.3 Catalytic activity and kinetics of ethylene hydrogenation

Ethylene hydrogenation is a crucial catalytic reaction that can be conducted under mild conditions and is widely employed as a probe reaction for extended metal surfaces and supported metal catalysts, including Pt, Ir, Rh, and Au. In this study, the catalytic performance of the 4 wt% $PdCl_2$@Py-1P COF catalyst and its respective pristine COF support was evaluated for ethylene hydrogenation at atmospheric pressure and a constant temperature of 22 °C.

Notably, in both the non-purified (0.35 wt% Pd impurity) and PPh_3-purified (0.23 wt% Pd impurity) samples, no significant difference in activity was observed between the Pd-loaded catalysts and their corresponding pristine COF supports. These findings suggest that, in the absence of complete purification, the majority of the observed activity originates from

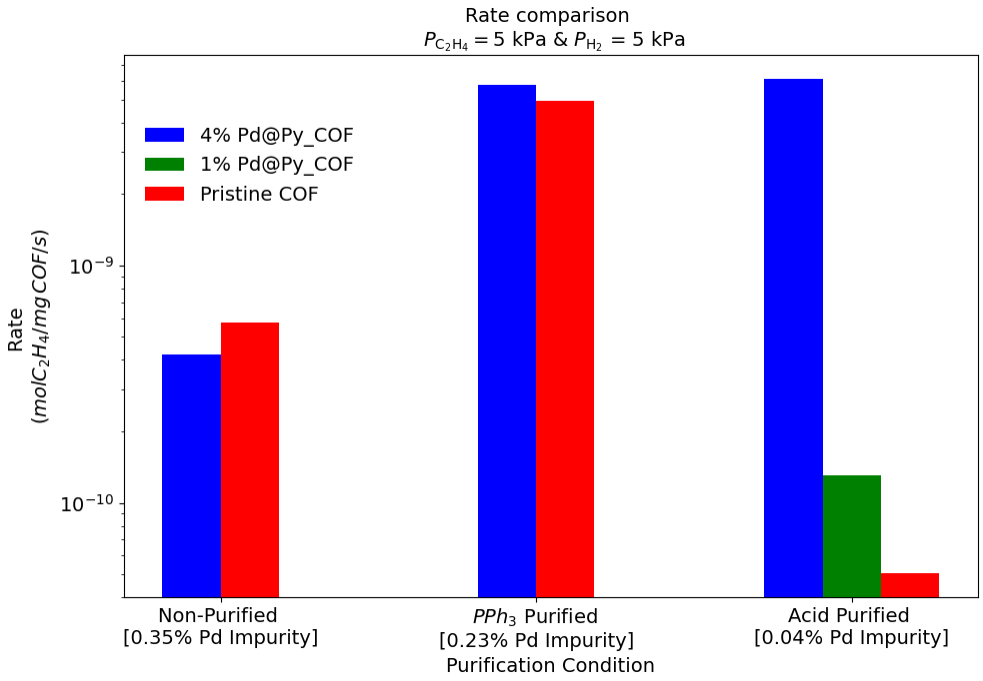

Figure 1.13: Comparison of reaction rate for different purification processes

the pristine COF, making it challenging to distinguish the catalytic contribution of inherent Pd impurities from that of the intentionally introduced Pd catalyst. However, despite the lower Pd impurity content in the PPh_3-purified COF compared to the non-purified COF, the former exhibited higher catalytic activity. This suggests that PPh_3 purification may reduce the size of Pd impurity clusters, thereby enhancing their catalytic performance. Acid purification, which effectively removes the majority of Pd impurities, led to a remarkable ~100-fold enhancement in catalytic activity for the 4 wt% Pd@Py-1P COF relative to the acid-purified pristine COF.

However, at higher Pd loadings, there is a possibility of single atoms aggregating under reaction conditions. To probe the catalyst structure during reaction, diffuse reflectance infrared Fourier transform spectroscopy (DRIFTS) of CO adsorption was performed following *in situ* ethylene hydrogenation (5 kPa C_2H_4 and 5 kPa H_2 in N_2 balance at 22 °C), as shown in Figure 1.14. A CO band at 1920 cm^{-1} [gray area] observed for the higher loading is attributed to bridge-bound CO on Pd clusters, suggesting that single atoms tend to form

clusters under reaction conditions. In contrast, at lower Pd loading, the CO adsorption feature indicated the presence of only atomically dispersed Pd sites under reaction conditions, highlighting the importance of monomer purification prior to COF synthesis and subsequent metal incorporation. Notably, even at 1 wt% Pd loading, acid-purified samples showed enhanced activity compared to the pristine COF, further confirming the effectiveness of the purification strategy.

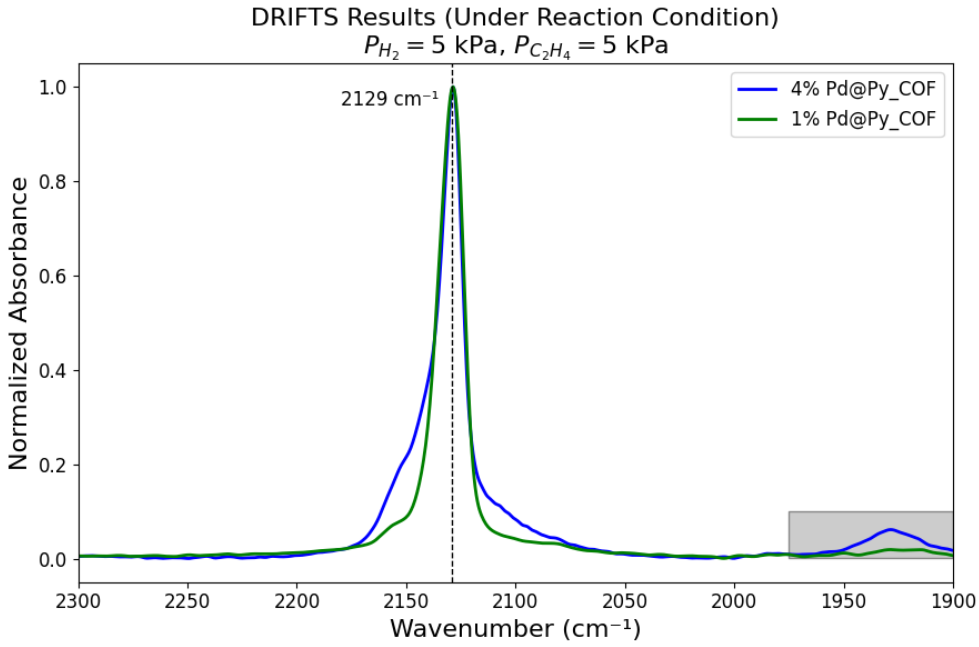

Figure 1.14: Normalized CO-DRIFTS spectra showing peak position at 2129 cm^{-1} and additional low-intensity features indicating Pd clustering.

The catalytic hydrogenation of ethylene has been extensively studied, with a well-established reaction pathway involving the sequential addition of atomic hydrogen across the carbon–carbon double bond [57]. Figure: 1.15 illustrates the dependence of turnover frequency (TOF) on the partial pressures of hydrogen and ethylene. The slopes of the best linear fits to the kinetic data under steady-state conditions reveal a reaction order of 0.57 with respect to hydrogen and approximately zero (1.00) with respect to ethylene. Similar kinetic behavior has been reported for ethylene hydrogenation over supported metal single atoms[58], subnanometer clusters[59, 60], and nanoparticles[57, 61]. Catalysts based on supported Ir[60,

62] and Rh [59, 63]have demonstrated activity under 353 K and atmospheric pressure, with hydrogen exhibiting a typical reaction order of approximately 0.5, and ethylene approaching zero. This trend suggests that ethylene adsorption is not rate-limiting, while hydrogen undergoes dissociative adsorption on the metal surface [64].

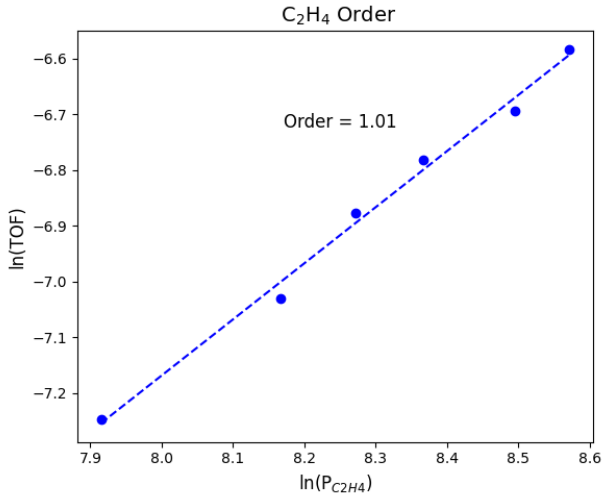

(a)

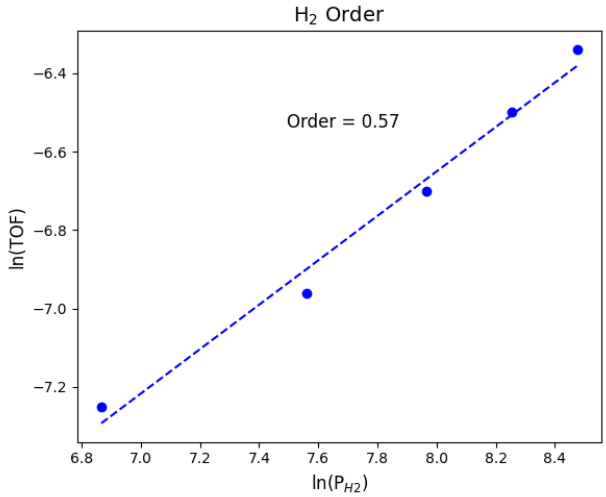

(b)

Figure 1.15: Kinetics of ethylene hydrogenation catalyzed by 1% Pd@Py-COF (a) Dependence of TOF on C_2H_4 partial pressure at a constant H_2 partial pressure of 5 kPa (the reaction order in ethylene is 1.01). (b) Dependence of TOF on H_2 partial pressure at a constant ethylene partial pressure of 5 kPa (the reaction order in H_2 is 0.57).

In the present study, the observed slightly positive reaction order with respect to ethy-

lene may indicate comparatively weaker ethylene adsorption on isolated Pd single atoms. The half-order dependence on hydrogen pressure at lower temperatures further implies that hydrogen adsorption is likely equilibrated under these conditions[65]. These findings suggest that at lower Pd loadings, where single atoms remain stable under reaction conditions, ethylene hydrogenation may proceed via a distinct reaction mechanism. However, a deeper understanding of the active site structure and the influence of chloride ligands is necessary to fully elucidate the catalytic behavior.

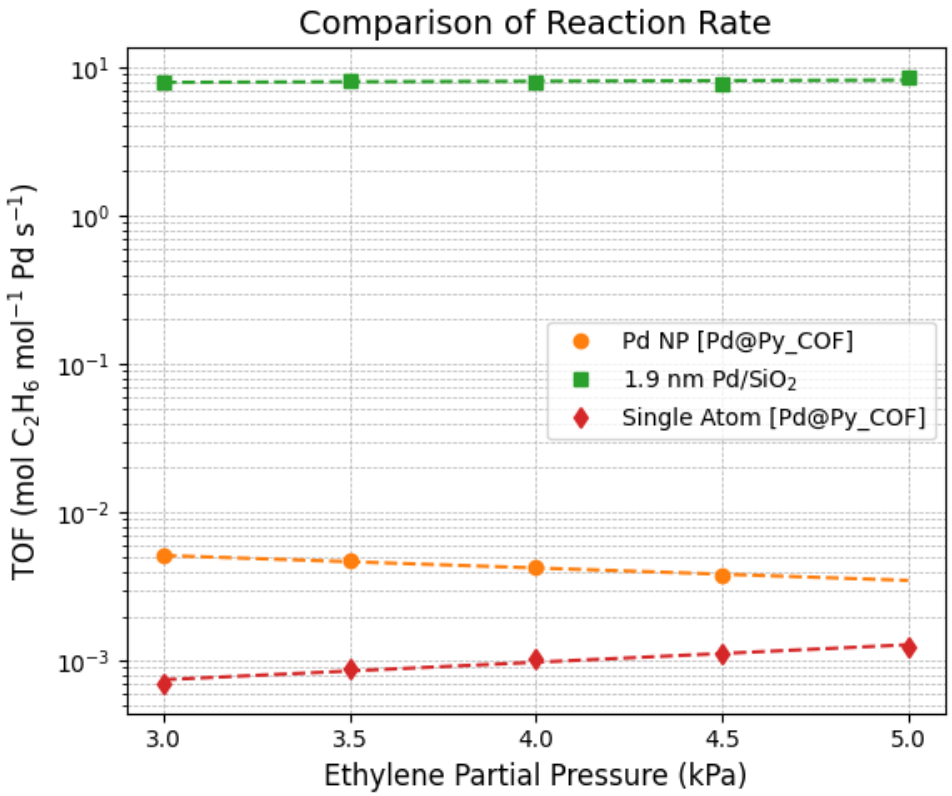

Figure 1.16: Reaction Rate comparsion between Pd single-atom and Pd nanoparticle

Figure 1.17 presents a comparison of ethylene hydrogenation rates over three different Pd-based catalyst systems—Pd single atoms supported on a COF, Pd nanoparticles on COF, and 1.9 nm Pd nanoparticles on SiO_2—as a function of ethylene partial pressure (3–5 kPa), under constant temperature and hydrogen pressure. The Pd single-atom catalyst exhibits significantly lower activity than both nanoparticle-based systems, which is attributed to the

weaker adsorption of ethylene on isolated Pd sites. The observed reaction kinetics suggest distinct mechanistic pathways for each catalyst. While the Pd single-atom system shows a slightly positive reaction order with respect to ethylene, the Pd nanoparticles on COF and SiO_2 exhibit near-zero and negative orders, respectively. The weak binding of ethylene on single atoms implies reduced surface coverage and minimal inhibition, suggesting that such sites may offer enhanced selectivity for acetylene semi-hydrogenation reactions.

1.5 Conclusion

The presence of palladium contamination originating from the synthesis of the PyTTA monomer significantly influences the performance of Pd single-atom catalysts (SACs) supported on the imine-linked Py-1P COF, highlighting the necessity of monomer purification. However, the choice of purification method not only affects impurity removal but also alters the physical properties of the resulting COF. These structural changes are evident in XRD patterns, SEM morphology, and pore size distributions. Both purification methods eliminate the characteristic XRD peak at 40°, which is attributed to Pd agglomeration in the unpurified Py-1P COF. SEM imaging reveals that acid column purification produces cleaner and more well-defined COF sheets compared to both the unpurified and PPh_3-purified samples. Although PPh_3 purification introduces structural defects, as detected by XPS, it also enhances catalytic activity relative to the unpurified COF, likely due to changes in the cluster size of residual Pd impurities. In contrast, acid purification preserves the original Pd–N coordination environment, allowing clear differentiation in activity between the 4 wt% Pd-loaded sample and the pristine COF. Notably, even at a reduced Pd loading of 1 wt%, which is important for maintaining catalyst stability under reaction conditions, the acid-purified sample exhibited significantly higher activity compared to the pristine COF. These findings underscore the critical role of purification in modulating the COF framework and the Pd coordination environment, both of which have a direct impact on catalyst performance and selectivity in ethylene and acetylene hydrogenation.

1.6 Future Plan

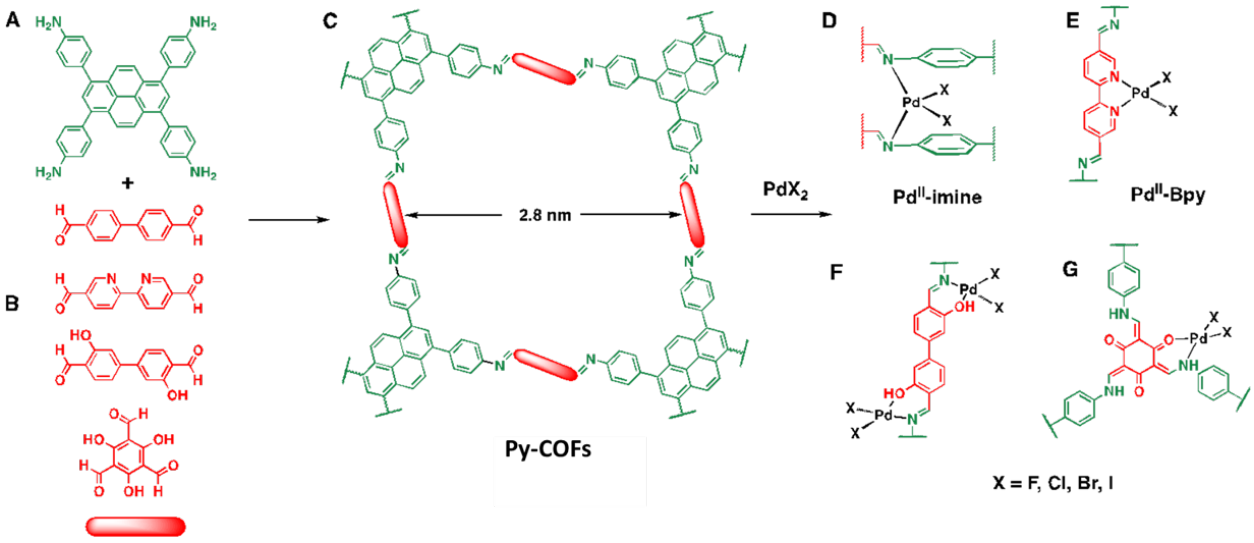

Figure 1.17: Future plan of this project

To further tune the catalytic performance of Pd-based single-atom catalysts supported on COFs, future efforts will focus on rationally modifying the framework structure by altering both the monomer and linker components. These modifications aim to systematically vary the coordination environment of the active sites, thereby changing the nature of the binding sites and metal ligands surrounding the Pd centers. Such changes are expected to directly influence the electron density at the Pd active site, which in turn could impact the catalyst's activity, stability, and selectivity, particularly for acetylene semi-hydrogenation.

A key question that arises is how the electronic structure of Pd—governed by its coordination environment—affects its interaction with reactants and intermediates, and how these interactions dictate the overall catalytic performance. Investigating these effects will involve exploring possible reaction mechanisms for acetylene semi-hydrogenation over differently coordinated Pd sites. This understanding will be essential to guide the design of next-generation COF-supported catalysts with enhanced selectivity and performance for in-

dustrially relevant hydrogenation processes.

Chapter 2:

Nanoparticle Size Effects on the Kinetics and Adsorbate-Induced Restructuring of Supported Pd_1Au_x Bimetallic Catalysts

Attribution:

This project was conducted in collaboration with Professor David Flaherty and graduate student Suchi Vijayaraghavan from Georgia Tech. Suchi Vijayaraghavan synthesized the catalyst and performed kinetic and other measurements (not discussed in this section). H.P.S. conducted the DRIFTS experiments. Professors Ayman Karim and David Flaherty jointly conceived the research idea, planned the experimental strategy, and supervised the overall project.

2.1 Introduction & Literature review

Catalysts composed of alloyed nanoparticles often demonstrate enhanced activity or selectivity compared to their monometallic counterparts. Notable examples of industrially relevant alloy catalysts include PdAg[66, 67] and PdPb[68] for alkyne semihydrogenation, PtSn for alkane dehydrogenation[69], PdAu for vinyl acetate monomer synthesis[70], and PtRh for simultaneous NO_x reduction and CO/hydrocarbon oxidation[71]. The improved catalytic performance of alloyed systems is frequently attributed to both electronic and geometric effects.[72] Electronic effects arise from changes in the electronic structure—such as d-band shifts—due to orbital rehybridization, charge transfer, or lattice strain induced by heteronuclear metal bonding.[73] Geometric effects, on the other hand, result from modifications to the atomic arrangement of active sites when a second metal disrupts the ensembles of contiguous atoms found in pure metals. These alterations can significantly influence the adsorption strength and configuration of catalytic intermediates.

Moreover, alloy surfaces typically expose multiple metallic elements with distinct binding affinities for reactants and intermediates. These differences in adsorption energetics can influence surface coverage and catalytic turnover. In some cases, disparities in adsorbate binding between alloy components can even lead to environment-induced restructuring. For example, Pd binds oxygen more strongly than Au, leading to Pd surface enrichment in PdAu nanoparticles under oxidative conditions[74], whereas inert or vacuum environments favor a more Au-rich surface composition. The size of PdAu bimetallic nanoparticles plays a crucial role in determining their surface structure and catalytic properties. As particle size decreases, the proportion of surface atoms increases dramatically. This increase in surface atom fraction enhances the availability of active sites for catalytic reactions. Smaller clusters not only exhibit a higher density of surface atoms but also interact with adsorbates differently, often leading to altered binding configurations and reactivity. These effects collectively facilitate dynamic surface restructuring, which is highly sensitive to changes in cluster size, compo-

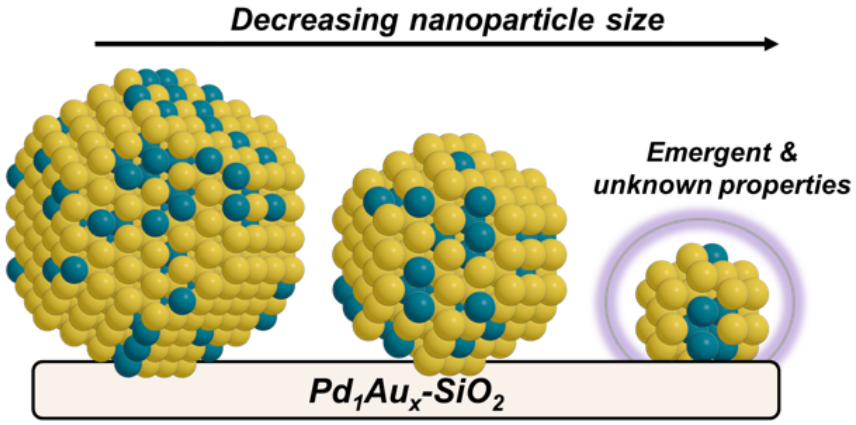

Figure 2.1: Size effects on PdAu bimetallic alloy

sition, and reaction conditions. Such restructuring can significantly influence the activity, selectivity, and stability of PdAu catalysts, emphasizing the importance of nanoscale control in catalyst design.

Alloy surfaces are inherently dynamic under reaction-relevant temperatures, and their surface composition and morphology can deviate significantly from the as-synthesized state. Such transformations may occur during annealing[75], pretreatment procedures[76], or even in situ under reaction conditions. For dilute Pd-in-Au systems, maintaining catalytically active Pd at the surface of an otherwise inert Au matrix is highly desirable. However, due to the higher surface free energy of Pd (2.05 J/m^2) relative to Au (1.63 J/m^2)[77], Pd tends to diffuse into the bulk under reducing environments, leading to surface depletion. Scanning tunneling microscopy (STM) studies have demonstrated that the distribution of Pd species on Au surfaces can be tuned through temperature-controlled deposition.[78] For instance, deposition of 1 atom % Pd on Au(111) at ∼300 K yields a mixture of Pd islands and smaller ensembles, whereas subsequent annealing at 450 K causes Pd to dissolve into the Au bulk. Notably, under reactive conditions, Pd can segregate back to the surface in the presence of strongly binding adsorbates such as CO and O_2.[76] These species preferentially adsorb onto Pd sites, effectively stabilizing Pd at the surface by lowering the overall surface free

energy.[79] CO-induced reverse segregation has been reported across several bimetallic systems, including Pd/Au(111)[80], Au/Pd(100)[81], and AuPt nanoparticles[82], highlighting the dynamic interplay between adsorbates and surface composition in alloy catalysts.

CO adsorption measured by DRIFTS (diffuse reflectance infrared Fourier transform spectroscopy) is a useful technique to characterize the surface of supported metal catalysts and has also been employed to study AuPd bimetallic catalysts. On pure Pd surfaces, CO preferentially adsorbs at bridge (μ_2-CO) and hollow (μ_3-CO) sites. However, in PdAu alloys, the disruption of these Pd ensembles shifts CO adsorption to atop (η^1-CO) sites, reflecting the significant influence of ensemble geometry on adsorbate binding.[83] Such behavior highlights how the interplay between electronic structure and atomic arrangement in alloy nanoparticles governs their catalytic performance.

2.2 Objective of the project

The overall objective of this project is to elucidate the structure–property relationships in Pd_1Au_x alloy nanoparticles by systematically varying nanoparticle size and palladium composition. The study aims to (1) develop controlled synthetic strategies for preparing PdAu bimetallic systems, (2) characterize their structural and electronic properties under reactive environments using advanced techniques such as transmission electron microscopy (TEM), CO-FTIR spectroscopy, and X-ray absorption spectroscopy (XAS), and (3) correlate these structural features with catalytic activity and thermodynamic behavior during hydrogen peroxide production.

Within this broader framework, the main focus of the thesis is on utilizing carbon monoxide diffuse reflectance infrared Fourier transform spectroscopy (CO-DRIFTS) to investigate the structural evolution of PdAu bimetallic catalysts under different adsorbates. Particular attention is given to how these structural changes vary as a function of particle size, composition, and temperature.

2.3 Experimental Procedures

2.3.1 Catalyst Preparation

The synthesis of Pd_1Au_x–SiO_2 catalysts begins with the preparation of the Au–bis(ethylenediamine) complex from a gold chloride precursor. This organometallic complexation step enables improved dispersion and charge control for subsequent adsorption. The resulting complex is then deposited onto a silica support via the Strong Electrostatic Adsorption (SEA) method, which relies on pH-tuned electrostatic interactions to anchor the gold species uniformly onto the surface. Following adsorption, the material is dried and reduced to form well-dispersed Au nanoparticles. Subsequently, palladium is introduced using an electroless deposition technique, allowing precise control over Pd loading and enabling the formation of Pd_1Au_x alloy nanoparticles. By varying the Pd precursor concentration during electroless deposition, a range of Pd compositions can be achieved, facilitating a systematic investigation of structure–property relationships as a function of particle size and alloying.

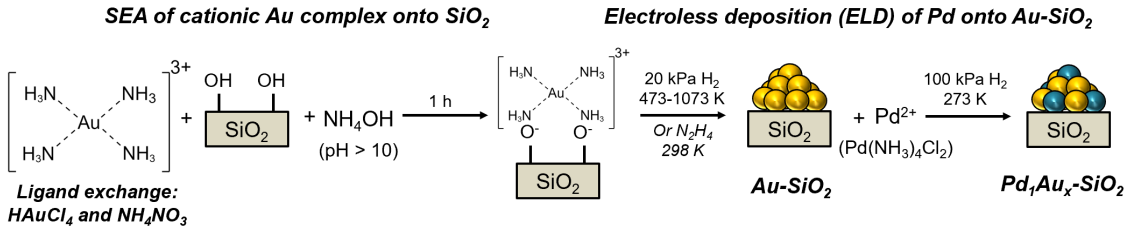

Figure 2.2: Synthesis process of PdAu bimetallic catalyst with different Pd loading

2.3.2 Catalyst Characterization

DRIFTS measurements of CO adsorption were carried out using a Thermo Fisher Scientific Nicolet iS50 FTIR spectrometer equipped with a liquid nitrogen-cooled mercury-cadmium-telluride (MCT) infrared detector. Carbon monoxide (CO) was used as a probe molecule due to its well-defined and sensitive vibrational features, which reflect the electronic and ge-

ometric structure of surface-active sites. Cryogenic temperatures were employed to suppress thermal motion and prevent CO-induced surface restructuring, ensuring reliable characterization of the catalyst's surface. Catalyst samples were loaded into an *in situ* Praying Mantis diffuse reflectance cell (Harrick Scientific Products) for analysis. Prior to CO exposure, all samples were reduced under 20 kPa of H_2 at 200 °C to generate a metallic state. The reduced samples were then cooled to –120 °C under different gas environments, including N_2, H_2, or O_2, depending on the pretreatment protocol. CO adsorption spectra were collected under 2 kPa CO, enabling evaluation of the structural dynamics of Pd-containing active sites under varying adsorbate conditions.

2.4 Results & Dicussions

2.4.1 Absorbates Effect

The DRIFTS spectra presented in the first row of Figure 2.3 illustrate CO adsorption on Au/SiO_2 following different pretreatment conditions. When the sample was cooled under N_2, a relatively broad peak centered at 2105 cm^{-1} was observed, accompanied by a minor shoulder at 2112 cm^{-1}. The broadness of the signal suggests the presence of multiple adsorption environments. According to literature, CO bands in the 2120–2080 cm^{-1} range are typically associated with adsorption on low-coordinated Au sites, such as steps or defects[84, 85], whereas bands in the 2080–2000 cm^{-1} region correspond to CO adsorption on negatively charged Au clusters [86, 87, 88, 89]. Higher-frequency bands (above 2120 cm^{-1}) are indicative of CO adsorption on positively charged Au species (Au^+), with bands beyond 2140 cm^{-1} corresponding to CO adsorbed on highly oxidized Au^{n+} ($n \geq 1$) sites [90, 91, 92, 93]. Upon cooling the Au/SiO_2 sample under H_2, the shoulder at 2112 cm^{-1} became the dominant feature, indicating subtle restructuring of the surface. In contrast, O_2 pretreatment resulted in a distinct blue shift of the CO stretching band to 2129 cm^{-1}. This shift suggests the formation of new adsorption sites due to interaction between the gold surface and pre-

adsorbed oxygen species. The emergence of this higher-frequency band is attributed to CO bound at gold step sites modified by reactive oxygen species such as superoxides or peroxides. These interactions likely result in structures such as O_2–Au^+–CO or $O^{\delta-}$–$Au^{\delta+}$–CO, consistent with electron transfer from the gold to the adsorbed oxygen[94].

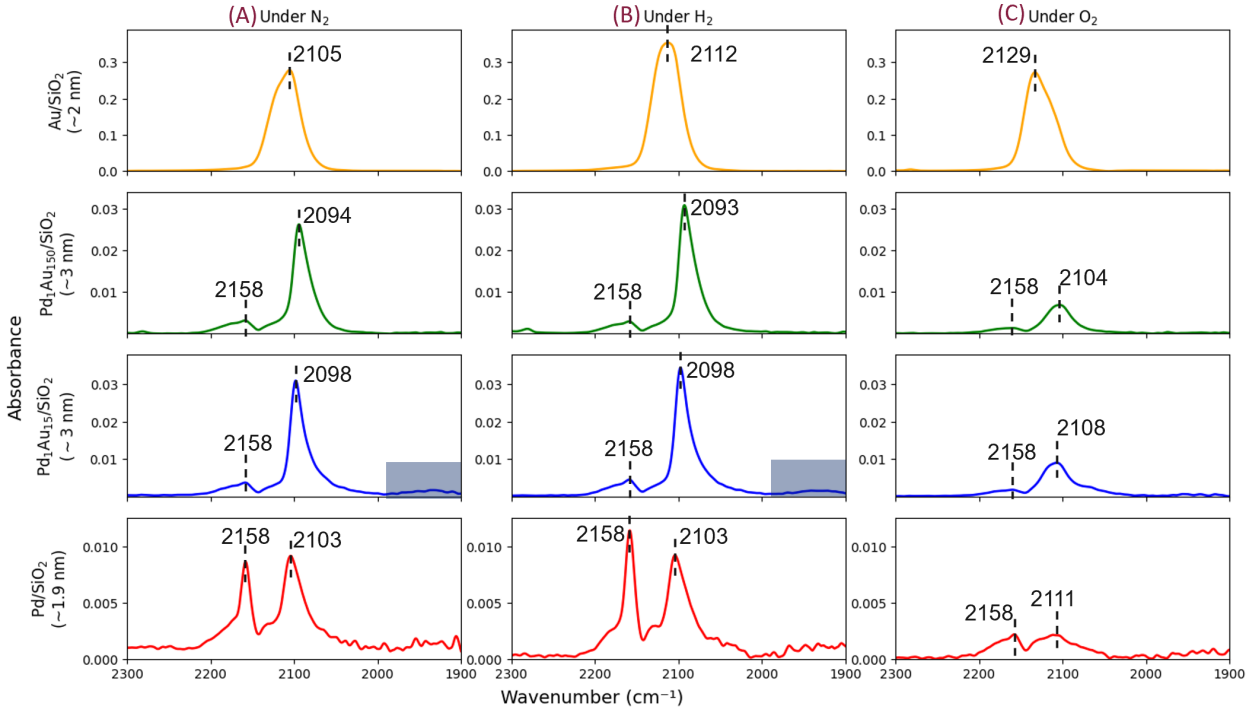

Figure 2.3: IR spectra for PdAu alloy under different adsorbates. All measurements were performed at −112 °C after a 5-minute N_2 flush, followed by 2 kPa CO adsorption.

The DRIFTS spectra of CO adsorption on Pd/SiO_2 (1.9 nm) reveal distinct features depending on the gas environment used during cooling. When cooled under N_2 and H_2, three prominent peaks are observed at 2158, 2131, and 2103 cm^{-1}. These can be assigned to CO adsorbed on Pd^{2+}, Pd^+, and metallic Pd^0 sites, respectively [95]. Notably, cooling under O_2 leads to a significant reduction in overall CO adsorption intensity, suggesting the pre-adsorbed oxygen may induce competitive adsorption, blocking CO access to active sites. A comparison of the peak positions between pure Pd and pure Au reveals that they are relatively close, making it challenging to confidently assign specific peaks in the PdAu bimetallic alloy.

For the PdAu bimetallic catalysts, the CO stretching frequencies remain relatively unchanged under N_2 and H_2 cooling conditions, indicating minimal structural or electronic alterations. However, under O_2 cooling, a noticeable reduction in peak intensity is observed. This behavior can be attributed to the stronger binding affinity of oxygen to Pd compared to Au, which results in surface enrichment of Pd atoms under oxidative conditions, especially relative to inert or vacuum environments [74]. In the case of the $PdAu_{15}/SiO_2$, a distinct feature in the 1900–2000 cm^{-1} region is observed, corresponding to bridge-bound CO on contiguous Pd sites. This feature is absent in the $PdAu_{150}/SiO_2$, suggesting a higher degree of Pd site isolation due to dilution by Au atoms.

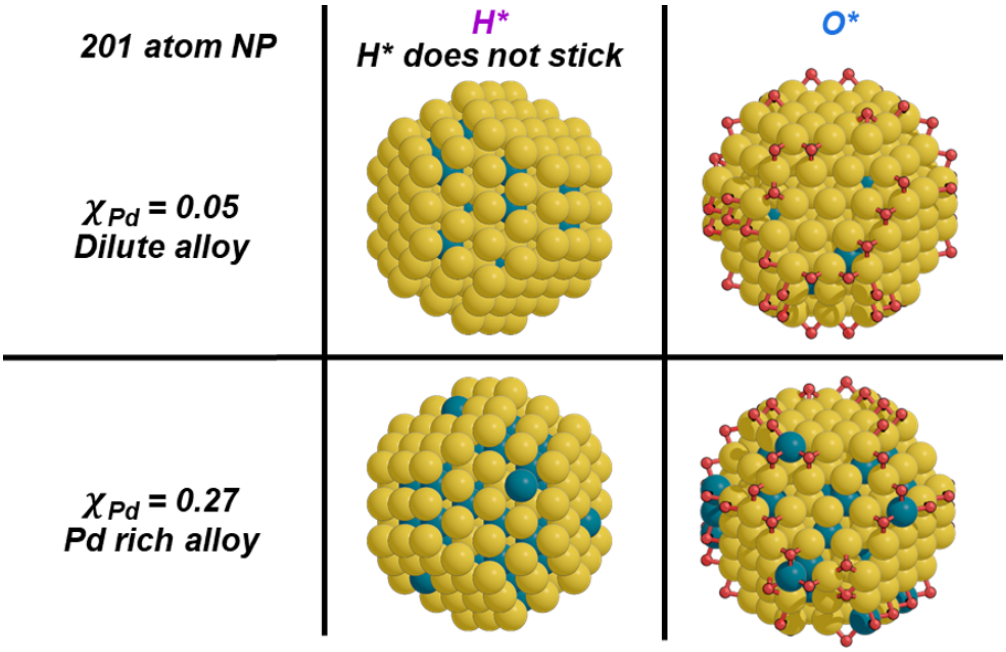

Figure 2.4: Restructuring behavior of PdAu alloy under H_2, O_2

2.4.2 Temperature Effect

Alloy surfaces are known to exhibit dynamic structural behavior under reaction-relevant temperatures. Compared to their as-synthesized state, significant changes in surface composition and morphology can occur as the temperature varies. Previous studies have reported such transformations at elevated temperatures, where, under CO-rich environments, Pd atoms

migrate to the surface of PdAu alloys ($\leq 150\,^{\circ}C$), replacing Au atoms and forming Pd–CO complexes [96]. Upon heating above 150 °C, CO desorbs, allowing Pd to reincorporate into the bulk, restoring the Pd–Au alloy structure [96]. However, observation of such structural rearrangements at cryogenic temperatures remains uncommon, making such findings particularly intriguing and significant since cryogenic temperature minimizes thermal mobility, preventing any CO-induced restructuring.

In this study, diffuse reflectance infrared Fourier transform spectroscopy (DRIFTS) was employed to monitor these structural changes. As the temperature was increased from cryogenic conditions, an enhanced absorption band emerged in the 1900–2000 cm^{-1} region, suggesting the formation of Pd ensembles species due to surface atom rearrangement Fig:2.5. This restructuring is primarily induced by the high CO coverage on Au, which facilitates the migration of subsurface Pd to the surface as the temperature increases from cryogenic conditions. A similar trend is observed at room temperature (25 °C), where low CO coverage on Au has minimal effect on Pd migration 2.6. In contrast, high CO coverage enhances the interaction with Au, promoting the emergence of Pd from the subsurface to the surface.

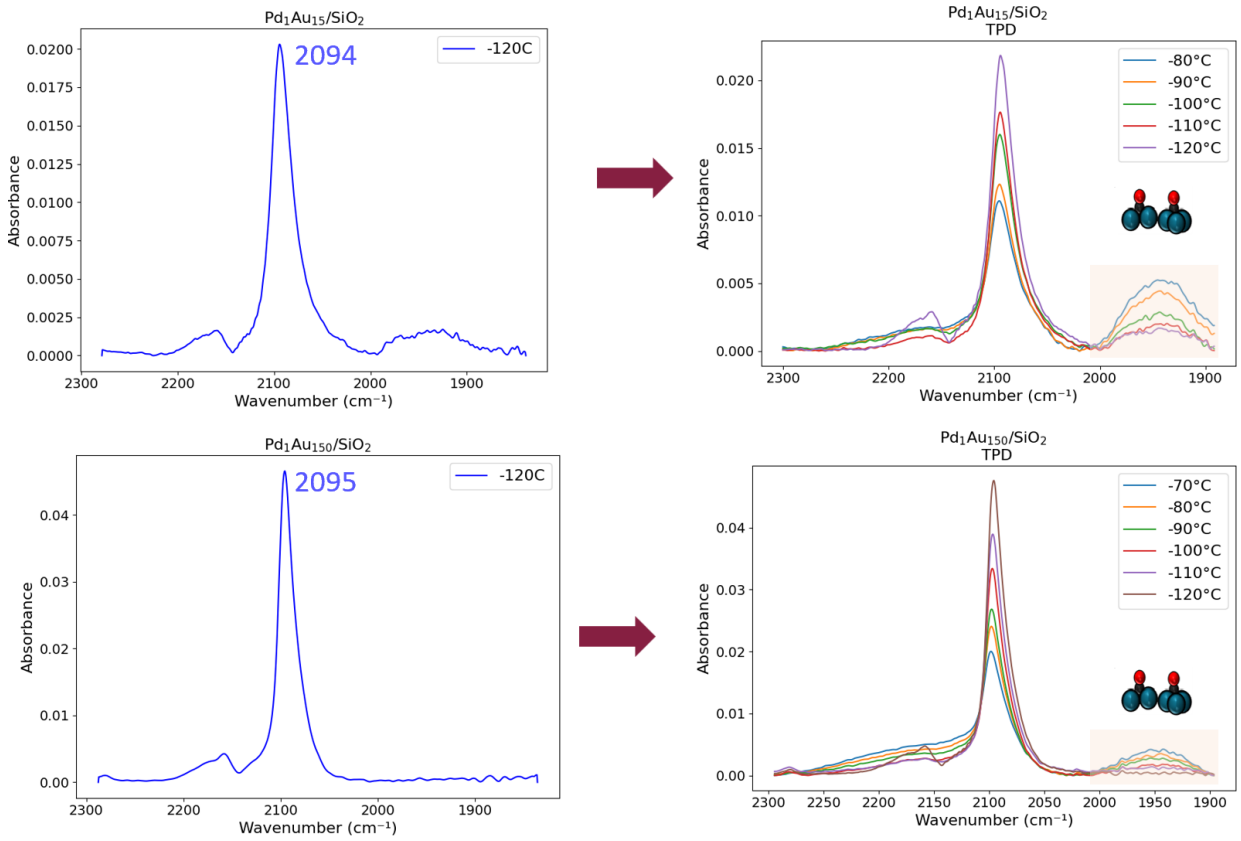

Figure 2.5: DRIFTS spectra showing CO adsorption on Pd_1Au_{15}/SiO_2 and Pd_1Au_{150}/SiO_2 at –120 °C (left), and their temperature-dependent evolution (right).

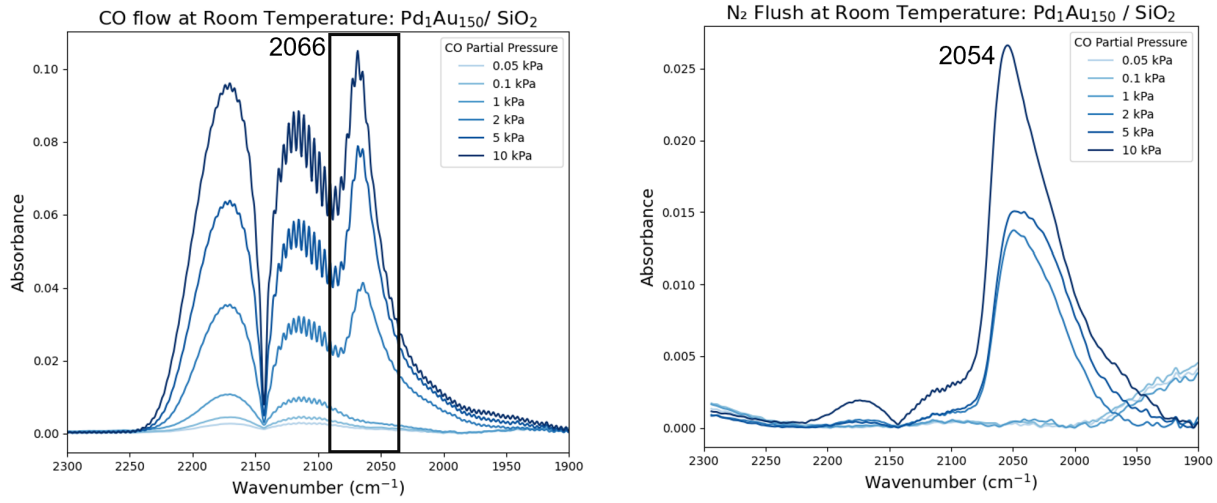

Figure 2.6: DRIFTS spectra showing CO adsorption on Pd_1Au_{15}/SiO_2 and Pd_1Au_{150}/SiO_2 at 25 °C (left), under 0.5-10 kPa CO partial paressure

Figure:2.7 illustrates the structural reversibility of PdAu alloys with different compositions as a function of temperature. At cryogenic temperature (−120 °C), a distinct CO absorption band appears at **2094 cm^{-1}** (blue), characteristic of CO linearly adsorbed on isolated Au atoms. Upon heating to room temperature (25 °C), this band shifts to **2052 cm^{-1}** (orange), indicating the formation of metallic Pd ensembles due to CO-induced Pd surface segregation. When the sample is re-cooled to cryogenic temperature (2nd run), the original CO band reappears at **2095 cm^{-1}** (green), signifying that Pd atoms migrate back into the bulk, restoring the initial single-atom dispersion. This reversible transformation highlights the dynamic nature of Pd surface distribution under varying thermal conditions and the role of CO in driving alloy restructuring.

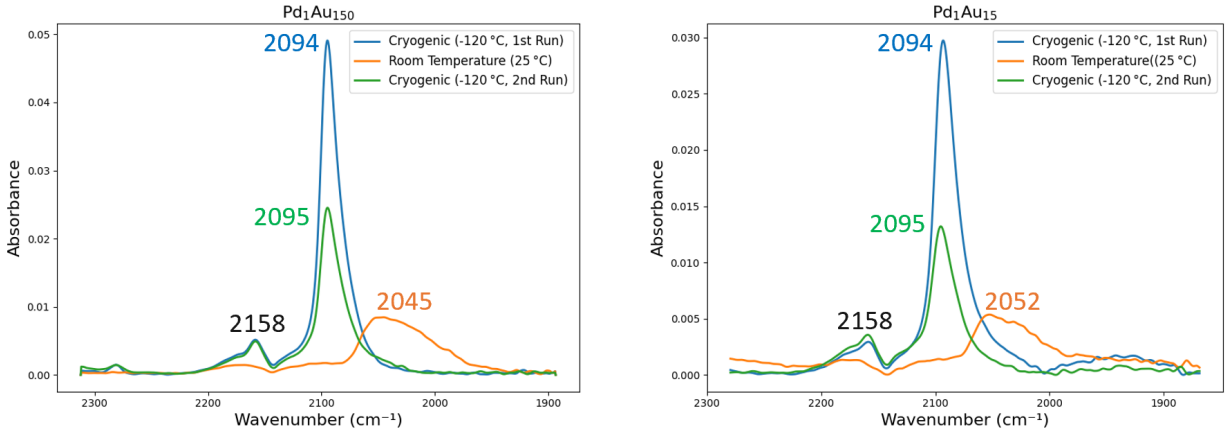

Figure 2.7: Reversible CO adsorption behavior on Pd_1Au_{150} and Pd_1Au_{15} observed via DRIFTS during temperature cycling between –120 °C and 25 °C.

2.5 Conclusion

This study offers a detailed investigation into the structural dynamics of PdAu bimetallic nanoparticles, examining how particle size, composition, adsorbate environment, and temperature collectively influence surface structure. Through the use of carbon monoxide as a probe molecule in DRIFTS analysis, we demonstrated that the degree and nature of Pd–Au surface restructuring are highly responsive to these variables. Our findings reveal that

strongly binding adsorbates, such as CO and O_2, promote Pd surface enrichment, whereas inert and reducing environments tend to stabilize Au-rich surfaces. Both large and small PdAu nanoparticles exhibit predominantly Au-rich surfaces. Importantly, we observed reversible structural changes in PdAu alloys at cryogenic temperatures—an uncommon finding in previous studies. This suggests that Pd surface segregation and re-incorporation are thermally driven and reversible, offering new insights into the dynamic nature of alloy surfaces under varying conditions. Overall, this work enhances the understanding of structure–property relationships in PdAu systems and highlights the effectiveness of operando spectroscopic techniques in probing active site environments. These insights are crucial for the rational design of bimetallic catalysts with improved stability, selectivity, and responsiveness in structure-sensitive reactions such as selective hydrogenation.

Bibliography

[1] Leilei Zhang, Maoxiang Zhou, Aiqin Wang, and Tao Zhang. Selective hydrogenation over supported metal catalysts: from nanoparticles to single atoms. *Chemical reviews*, 120(2):683–733, 2019.

[2] A Sarkany, Z Zsoldos, B Furlong, JW Hightower, and L Guczi. Hydrogenation of 1-butene and 1, 3-butadiene mixtures over pd/zno catalysts. *Journal of Catalysis*, 141(2):566–582, 1993.

[3] BM Collins. Selective hydrogenation of highly unsaturated hydrocarbons in the presence of less unsaturated hydrocarbons. Technical report, 1978.

[4] Noemí S Schbib, Miguel A García, Carlos E Gígola, and Alberto F Errazu. Kinetics of front-end acetylene hydrogenation in ethylene production. *Industrial & engineering chemistry research*, 35(5):1496–1505, 1996.

[5] ANR Bos and KR Westerterp. Mechanism and kinetics of the selective hydrogenation of ethyne and ethene. *Chemical engineering and processing: process intensification*, 32(1):1–7, 1993.

[6] Gianvito Vilé, Davide Albani, Neyvis Almora-Barrios, Núria López, and Javier Pérez-Ramírez. Advances in the design of nanostructured catalysts for selective hydrogenation. *ChemCatChem*, 8(1):21–33, 2016.

[7] Robert AW Johnstone, Anna H Wilby, and Ian D Entwistle. Heterogeneous catalytic transfer hydrogenation and its relation to other methods for reduction of organic compounds. *Chemical Reviews*, 85(2):129–170, 1985.

[8] Maria J Climent, Avelino Corma, and Sara Iborra. Heterogeneous catalysts for the one-pot synthesis of chemicals and fine chemicals. *Chemical Reviews*, 111(2):1072–1133, 2011.

[9] Petr Kluson and Libor Cerveny. Selective hydrogenation over ruthenium catalysts. *Applied Catalysis A: General*, 128(1):13–31, 1995.

[10] Carolyn A Schoenbaum, Daniel K Schwartz, and J Will Medlin. Controlling the surface environment of heterogeneous catalysts using self-assembled monolayers. *Accounts of Chemical Research*, 47(4):1438–1445, 2014.

[11] Gianvito Vilé, Neyvis Almora-Barrios, Sharon Mitchell, Núria López, and Javier Pérez-Ramírez. From the lindlar catalyst to supported ligand-modified palladium nanoparticles: selectivity patterns and accessibility constraints in the continuous-flow three-phase hydrogenation of acetylenic compounds. *Chemistry–A European Journal*, 20(20):5926–5937, 2014.

[12] Wenxin Niu, Yongjun Gao, Weiqing Zhang, Ning Yan, and Xianmao Lu. Pd–pb alloy nanocrystals with tailored composition for semihydrogenation: taking advantage of catalyst poisoning. *Angewandte Chemie*, 127(28):8389–8392, 2015.

[13] Helv Lindlar. Ein neuer katalysator für selektive hydrierungen. *Helvetica Chimica Acta*, 35(2):446–450, 1952.

[14] Andrzej Borodziński and Geoffrey C Bond. Selective hydrogenation of ethyne in ethene-rich streams on palladium catalysts. part 1. effect of changes to the catalyst during reaction. *Catalysis Reviews*, 48(02):91–144, 2006.

[15] Felix Studt, Frank Abild-Pedersen, Thomas Bligaard, Rasmus Z Sørensen, Claus H Christensen, and Jens K Nørskov. Identification of non-precious metal alloy catalysts for selective hydrogenation of acetylene. *Science*, 320(5881):1320–1322, 2008.

[16] Detre Teschner, János Borsodi, Attila Wootsch, Zsolt Révay, Michael Havecker, Axel Knop-Gericke, S David Jackson, and Robert Schlögl. The roles of subsurface carbon and hydrogen in palladium-catalyzed alkyne hydrogenation. *Science*, 320(5872):86–89, 2008.

[17] Micaela Crespo-Quesada, Fernando Cárdenas-Lizana, Anne-Laure Dessimoz, and Lioubov Kiwi-Minsker. Modern trends in catalyst and process design for alkyne hydrogenations. *Acs Catalysis*, 2(8):1773–1786, 2012.

[18] A Sárkány, AH Weiss, and L Guczi. Structure sensitivity of acetylene-ethylene hydrogenation over pd catalysts. *J. Catal.;(United States)*, 98(2), 1986.

[19] Marina Ruta, Natalia Semagina, and Lioubov Kiwi-Minsker. Monodispersed pd nanoparticles for acetylene selective hydrogenation: particle size and support effects. *The Journal of Physical Chemistry C*, 112(35):13635–13641, 2008.

[20] Matthias Bauer, Roland Schoch, Lidong Shao, Bingsen Zhang, Axel Knop-Gericke, Marc Willinger, Robert Schlögl, and Detre Teschner. Structure–activity studies on highly active palladium hydrogenation catalysts by x-ray absorption spectroscopy. *The Journal of Physical Chemistry C*, 116(42):22375–22385, 2012.

[21] Yueqiang Cao, Wenzhao Fu, Zhijun Sui, Xuezhi Duan, De Chen, and Xinggui Zhou. Kinetics insights and active sites discrimination of pd-catalyzed selective hydrogenation of acetylene. *Industrial & Engineering Chemistry Research*, 58(5):1888–1895, 2019.

[22] Yufei He, Jiaxuan Fan, Junting Feng, Chiying Luo, Pengfei Yang, and Dianqing Li. Pd nanoparticles on hydrotalcite as an efficient catalyst for partial hydrogenation of acetylene: Effect of support acidic and basic properties. *Journal of Catalysis*, 331:118–127, 2015.

[23] Samane Komeili, Maryam Takht Ravanchi, and Abbas Taeb. The influence of alumina

phases on the performance of the pd–ag/al2o3 catalyst in tail-end selective hydrogenation of acetylene. *Applied Catalysis A: General*, 502:287–296, 2015.

[24] Alan J McCue and James A Anderson. Recent advances in selective acetylene hydrogenation using palladium containing catalysts. *Frontiers of Chemical Science and Engineering*, 9:142–153, 2015.

[25] Andrzej Borodziński and Andrzej Cybulski. The kinetic model of hydrogenation of acetylene–ethylene mixtures over palladium surface covered by carbonaceous deposits. *Applied Catalysis A: General*, 198(1-2):51–66, 2000.

[26] Jian Zhang, Zhijun Sui, Yi-An Zhu, De Chen, Xinggui Zhou, and Weikang Yuan. Composition of the green oil in hydrogenation of acetylene over a commercial pd-ag/al2o3 catalyst. *Chemical Engineering & Technology*, 39(5):865–873, 2016.

[27] Elaheh Esmaeili, Ali Morad Rashidi, Yadollah Mortazavi, Abbas Ali Khodadadi, and Mehdi Rashidzadeh. Smfs-supported pd nanocatalysts in selective acetylene hydrogenation: Pore structure-dependent deactivation mechanism. *Journal of energy chemistry*, 22(5):717–725, 2013.

[28] Yueqiang Cao, Zhijun Sui, Yian Zhu, Xinggui Zhou, and De Chen. Selective hydrogenation of acetylene over pd-in/al2o3 catalyst: promotional effect of indium and composition-dependent performance. *ACS Catalysis*, 7(11):7835–7846, 2017.

[29] G Hamm, T Schmidt, J Breitbach, D Franke, Conrad Becker, and Klaus Wandelt. The adsorption of ethene on pd (111) and ordered sn/pd (111) surface alloys. *Zeitschrift für Physikalische Chemie*, 223(1-2):209–232, 2009.

[30] Timothy Lear, Robert Marshall, J Antonio Lopez-Sanchez, S David Jackson, Thomas M Klapötke, Marcus Bäumer, Günther Rupprechter, Hans-Joachim Freund, and David Lennon. The application of infrared spectroscopy to probe the surface morphology of alumina-supported palladium catalysts. *The Journal of chemical physics*, 123(17), 2005.

[31] Mingshi Li and Jianyi Shen. Microcalorimetric studies of o2 and c2h4 adsorption on pd/sio2 catalysts modified by cu and ag. *Thermochimica acta*, 379(1-2):45–50, 2001.

[32] Xiao Feng, Xuesong Ding, and Donglin Jiang. Covalent organic frameworks. *Chemical Society Reviews*, 41(18):6010–6022, 2012.

[33] Adrien P Cote, Hani M El-Kaderi, Hiroyasu Furukawa, Joseph R Hunt, and Omar M Yaghi. Reticular synthesis of microporous and mesoporous 2d covalent organic frameworks. *Journal of the American Chemical Society*, 129(43):12914–12915, 2007.

[34] Shun Wan, Jia Guo, Jangbae Kim, Hyotcherl Ihee, and Donglin Jiang. A photoconductive covalent organic framework: self-condensed arene cubes composed of eclipsed 2d polypyrene sheets for photocurrent generation. *Angewandte Chemie International Edition*, 48(30):5439–5442, 2009.

[35] Eric L Spitler, Brian T Koo, Jennifer L Novotney, John W Colson, Fernando J Uribe-Romo, Gregory D Gutierrez, Paulette Clancy, and William R Dichtel. A 2d covalent organic framework with 4.7-nm pores and insight into its interlayer stacking. *Journal of the American Chemical Society*, 133(48):19416–19421, 2011.

[36] Fernando J Uribe-Romo, Christian J Doonan, Hiroyasu Furukawa, Kounosuke Oisaki, and Omar M Yaghi. Crystalline covalent organic frameworks with hydrazone linkages. *Journal of the American Chemical Society*, 133(30):11478–11481, 2011.

[37] David N Bunck and William R Dichtel. Bulk synthesis of exfoliated two-dimensional polymers using hydrazone-linked covalent organic frameworks. *Journal of the American Chemical Society*, 135(40):14952–14955, 2013.

[38] Adrien P Cote, Annabelle I Benin, Nathan W Ockwig, Michael O'Keeffe, Adam J Matzger, and Omar M Yaghi. Porous, crystalline, covalent organic frameworks. *science*, 310(5751):1166–1170, 2005.

[39] Misbah Shahid, Aziz ur Rehman, Tayyaba Najam, Hammad Majeed, Marwan Shalash, Salah M El-Bahy, Muhammad Sufyan Javed, Syed Shoaib Ahmad Shah, and Muhammad Altaf Nazir. Covalent organic frameworks: Synthesis and applications for photocatalysis. *ChemPhotoChem*, 8(10):e202400131, 2024.

[40] Di Meng, Jing Xue, Yufan Zhang, Tianjiao Liu, Chuncheng Chen, Wenjing Song, and Jincai Zhao. Covalent organic frameworks editing for efficient metallaphotoredox catalytic carbon–oxygen cross coupling of aryl halides with alcohols. *Catalysis Science & Technology*, 13(5):1518–1526, 2023.

[41] Hani M El-Kaderi, Joseph R Hunt, José L Mendoza-Cortés, Adrien P Côté, Robert E Taylor, Michael O'Keeffe, and Omar M Yaghi. Designed synthesis of 3d covalent organic frameworks. *Science*, 316(5822):268–272, 2007.

[42] MM Trandafir, L Pop, ND Hădade, M Florea, F Neațu, CM Teodorescu, B Duraki, Jeroen A van Bokhoven, I Grosu, Vasile I Pârvulescu, et al. An adamantane-based cof: stability, adsorption capability, and behaviour as a catalyst and support for pd and au for the hydrogenation of nitrostyrene. *Catalysis Science & Technology*, 6(23):8344–8354, 2016.

[43] Christian S Diercks and Omar M Yaghi. The atom, the molecule, and the covalent organic framework. *Science*, 355(6328):eaal1585, 2017.

[44] José L Segura, María J Mancheño, and Félix Zamora. Covalent organic frameworks based on schiff-base chemistry: synthesis, properties and potential applications. *Chemical Society Reviews*, 45(20):5635–5671, 2016.

[45] San-Yuan Ding, Jia Gao, Qiong Wang, Yuan Zhang, Wei-Guo Song, Cheng-Yong Su, and Wei Wang. Construction of covalent organic framework for catalysis: Pd/cof-lzu1 in suzuki–miyaura coupling reaction. *Journal of the American Chemical Society*, 133(49):19816–19822, 2011.

[46] Pradip Pachfule, Manas K Panda, Sharath Kandambeth, SM Shivaprasad, David Díaz Díaz, and Rahul Banerjee. Multifunctional and robust covalent organic framework–nanoparticle hybrids. *Journal of Materials Chemistry A*, 2(21):7944–7952, 2014.

[47] Pradip Pachfule, Sharath Kandambeth, David Díaz Díaz, and Rahul Banerjee. Highly stable covalent organic framework–au nanoparticles hybrids for enhanced activity for nitrophenol reduction. *Chemical Communications*, 50(24):3169–3172, 2014.

[48] Songlin Chao, Qingxin Guan, and Wei Li. Study of the active site for acetylene hydrochlorination in aucl3/c catalysts. *Journal of Catalysis*, 330:273–279, 2015.

[49] Yun-Nan Gong, Wenhui Zhong, Yang Li, Yunze Qiu, Lirong Zheng, Jun Jiang, and Hai-Long Jiang. Regulating photocatalysis by spin-state manipulation of cobalt in covalent organic frameworks. *Journal of the American Chemical Society*, 142(39):16723–16731, 2020.

[50] Harshitha Barike Aiyappa, Jayshri Thote, Digambar Balaji Shinde, Rahul Banerjee, and Sreekumar Kurungot. Cobalt-modified covalent organic framework as a robust water oxidation electrocatalyst. *Chemistry of Materials*, 28(12):4375–4379, 2016.

[51] Wanfu Zhong, Rongjian Sa, Liuyi Li, Yajun He, Lingyun Li, Jinhong Bi, Zanyong Zhuang, Yan Yu, and Zhigang Zou. A covalent organic framework bearing single ni sites as a synergistic photocatalyst for selective photoreduction of co2 to co. *Journal of the American Chemical Society*, 141(18):7615–7621, 2019.

[52] Qi Sun, Briana Aguila, Jason Perman, Nicholas Nguyen, and Shengqian Ma. Flexibility matters: cooperative active sites in covalent organic framework and threaded ionic polymer. *Journal of the American Chemical Society*, 138(48):15790–15796, 2016.

[53] Linus Stegbauer, Katharina Schwinghammer, and Bettina V Lotsch. A hydrazone-based covalent organic framework for photocatalytic hydrogen production. *Chemical Science*, 5(7):2789–2793, 2014.

[54] Pillaiyar Puthiaraj, Yu-Ri Lee, Siqian Zhang, and Wha-Seung Ahn. Triazine-based covalent organic polymers: design, synthesis and applications in heterogeneous catalysis. *Journal of Materials Chemistry A*, 4(42):16288–16311, 2016.

[55] Miao Guo, Sanjeevi Jayakumar, Mengfei Luo, Xiangtao Kong, Chunzhi Li, He Li, Jian Chen, and Qihua Yang. The promotion effect of π-π interactions in pd nps catalysed selective hydrogenation. *Nature Communications*, 13(1):1770, 2022.

[56] Chengjun Kang, Zhaoqiang Zhang, Vanessa Wee, Adam K Usadi, David C Calabro, Lisa Saunders Baugh, Shun Wang, Yuxiang Wang, and Dan Zhao. Interlayer shifting in two-dimensional covalent organic frameworks. *Journal of the American Chemical Society*, 142(30):12995–13002, 2020.

[57] H Molero, D Stacchiola, and WT Tysoe. The kinetics of ethylene hydrogenation catalyzed by metallic palladium. *Catalysis letters*, 101:145–149, 2005.

[58] Javier Guzman and Bruce C Gates. A mononuclear gold complex catalyst supported on mgo: spectroscopic characterization during ethylene hydrogenation catalysis. *Journal of Catalysis*, 226(1):111–119, 2004.

[59] Erjia Guan and Bruce C Gates. Stable rhodium pair sites on mgo: influence of ligands and rhodium nuclearity on catalysis of ethylene hydrogenation and h–d exchange in the reaction of h2 with d2. *ACS Catalysis*, 8(1):482–487, 2018.

[60] Erjia Guan, Louise Debefve, Monica Vasiliu, Shengjie Zhang, David A Dixon, and Bruce C Gates. Mgo-supported iridium metal pair-site catalysts are more active and resistant to co poisoning than analogous single-site catalysts for ethylene hydrogenation and hydrogen–deuterium exchange. *ACS Catalysis*, 9(10):9545–9553, 2019.

[61] Axel Binder, Martin Seipenbusch, Martin Muhler, and Gerhard Kasper. Kinetics and particle size effects in ethene hydrogenation over supported palladium catalysts at atmospheric pressure. *Journal of Catalysis*, 268(1):150–155, 2009.

[62] Christian Schöttle, Erjia Guan, Alexander Okrut, Nicolás A Grosso-Giordano, Andrew Palermo, Andrew Solovyov, Bruce C Gates, and Alexander Katz. Bulky calixarene ligands stabilize supported iridium pair-site catalysts. *Journal of the American Chemical Society*, 141(9):4010–4015, 2019.

[63] Varinia Bernales, Dong Yang, Jun Yu, Gamze Gumuslu, Christopher J Cramer, Bruce C Gates, and Laura Gagliardi. Molecular rhodium complexes supported on the metal-oxide-like nodes of metal organic frameworks and on zeolite hy: Catalysts for ethylene hydrogenation and dimerization. *ACS Applied Materials & Interfaces*, 9(39):33511–33520, 2017.

[64] Chun-Te Kuo, Yubing Lu, Pezhman Arab, K Shamara Weeraratne, Hani El-Kaderi, and Ayman M Karim. 18.1% single palladium atom catalysts on mesoporous covalent organic framework for gas phase hydrogenation of ethylene. *Cell Reports Physical Science*, 2(7), 2021.

[65] Scott A Goddard, Randy D Cortright, and JA Dumesic. Deuterium tracing studies and microkinetic analysis of ethylene hydrogenation over platinum. *Journal of Catalysis*, 137(1):186–198, 1992.

[66] Guang Xian Pei, Xiao Yan Liu, Aiqin Wang, Adam F Lee, Mark A Isaacs, Lin Li, Xiaoli Pan, Xiaofeng Yang, Xiaodong Wang, Zhijun Tai, et al. Ag alloyed pd single-atom catalysts for efficient selective hydrogenation of acetylene to ethylene in excess ethylene. *Acs Catalysis*, 5(6):3717–3725, 2015.

[67] Felix Studt, Frank Abild-Pedersen, Thomas Bligaard, Rasmus Z Sørensen, Claus H Christensen, and Jens K Nørskov. On the role of surface modifications of palladium catalysts in the selective hydrogenation of acetylene. *Angewandte Chemie*, 120(48):9439–9442, 2008.

[68] W Palczewska, A Jabłonski, Z Kaszkur, G Zuba, and J Wernisch. Study on lead

additives in modified palladium catalysts. *Journal of molecular catalysis*, 25(1-3):307–316, 1984.

[69] Vladimir Galvita, Georges Siddiqi, Pingping Sun, and Alexis T Bell. Ethane dehydrogenation on pt/mg (al) o and ptsn/mg (al) o catalysts. *Journal of Catalysis*, 271(2):209–219, 2010.

[70] Mingshu Chen, Dheeraj Kumar, Cheol-Woo Yi, and D Wayne Goodman. The promotional effect of gold in catalysis by palladium-gold. *Science*, 310(5746):291–293, 2005.

[71] Michael J D'Aniello Jr, David R Monroe, Constance J Carr, and Martin H Krueger. The redispersion of sintered pt, rh, and ptrh catalysts. *Journal of Catalysis*, 109(2):407–422, 1988.

[72] Vladimir Ponec. Alloy catalysts: the concepts. *Applied Catalysis A: General*, 222(1-2):31–45, 2001.

[73] Bjørk Hammer and Jens Kehlet Nørskov. Theoretical surface science and catalysis—calculations and concepts. In *Advances in catalysis*, volume 45, pages 71–129. Elsevier, 2000.

[74] Hazar Guesmi, Catherine Louis, and Laurent Delannoy. Chemisorbed atomic oxygen inducing pd segregation in pdau (1 1 1) alloy: Energetic and electronic dft analysis. *Chemical Physics Letters*, 503(1-3):97–100, 2011.

[75] Jin Soo Lim, Jonathan Vandermause, Matthijs A Van Spronsen, Albert Musaelian, Yu Xie, Lixin Sun, Christopher R O'Connor, Tobias Egle, Nicola Molinari, Jacob Florian, et al. Evolution of metastable structures at bimetallic surfaces from microscopy and machine-learning molecular dynamics. *Journal of the American Chemical Society*, 142(37):15907–15916, 2020.

[76] Matthijs A van Spronsen, Kaining Daunmu, Christopher R O'Connor, Tobias Egle, Heath Kersell, Judit Oliver-Meseguer, Miquel B Salmeron, Robert J Madix, Philippe Sautet, and Cynthia M Friend. Dynamics of surface alloys: rearrangement of pd/ag (111) induced by co and o2. *The Journal of Physical Chemistry C*, 123(13):8312–8323, 2018.

[77] William R Tyson and William Alfred Miller. Surface free energies of solid metals: Estimation from liquid surface tension measurements. *Surface Science*, 62(1):267–276, 1977.

[78] Ashleigh E Baber, Heather L Tierney, Timothy J Lawton, and E Charles H Sykes. An atomic-scale view of palladium alloys and their ability to dissociate molecular hydrogen. *ChemCatChem*, 3(3):607–614, 2011.

[79] Feng Tao, Michael E Grass, Yawen Zhang, Derek R Butcher, James R Renzas, Zhi Liu, Jen Y Chung, Bongjin S Mun, Miquel Salmeron, and Gabor A Somorjai. Reaction-driven restructuring of rh-pd and pt-pd core-shell nanoparticles. *Science*, 322(5903):932–934, 2008.

[80] A Piednoir, MA Languille, L Piccolo, A Valcarcel, FJ Cadete Santos. Aires, and JC Bertolini. Pd (111) versus pd–au (111) in carbon monoxide oxidation under elevated pressures. *Catalysis letters*, 114:110–114, 2007.

[81] Zhenjun Li, Feng Gao, Octavio Furlong, and Wilfred T Tysoe. Adsorption of carbon monoxide au/pd (1 0 0) alloys in ultrahigh vacuum: Identification of adsorption sites. *Surface science*, 604(2):136–143, 2010.

[82] Rachel P Doherty, Jean-Marc Krafft, Christophe Méthivier, Sandra Casale, Hynd Remita, Catherine Louis, and Cyril Thomas. On the promoting effect of au on co oxidation kinetics of au–pt bimetallic nanoparticles supported on sio2: An electronic effect? *Journal of Catalysis*, 287:102–113, 2012.

[83] EL Kugler and M Boudart. Ligand and ensemble effects in the adsorption of carbon monoxide on supported palladium-gold alloys. *Journal of Catalysis*, 59(2):201–210, 1979.

[84] Y. Jugnet, F.J. Cadete Santos Aires, C. Deranlot, L. Piccolo, and J.C. Bertolini. Co chemisorption on au(110) investigated under elevated pressures by polarized reflection absorption infrared spectroscopy and scanning tunneling microscopy. *Surface Science*, 521(1):L639–L644, 2002.

[85] Douglas C Meier, V Bukhtiyarov, and D Wayne Goodman. Co adsorption on au (110)-(1× 2): An iras investigation. *The Journal of Physical Chemistry B*, 107(46):12668–12671, 2003.

[86] T Tabakova, Flora Boccuzzi, Maela Manzoli, JW Sobczak, V Idakiev, and D Andreeva. Effect of synthesis procedure on the low-temperature wgs activity of au/ceria catalysts. *Applied Catalysis B: Environmental*, 49(2):73–81, 2004.

[87] FC Meunier, Alexandre Goguet, Christopher Hardacre, Robbie Burch, and D Thompsett. Quantitative drifts investigation of possible reaction mechanisms for the water–gas shift reaction on high-activity pt-and au-based catalysts. *Journal of Catalysis*, 252(1):18–22, 2007.

[88] H Daly, J Ni, D Thompsett, and FC Meunier. On the usefulness of carbon isotopic exchange for the operando analysis of metal–carbonyl bands by ir over ceria-containing catalysts. *Journal of Catalysis*, 254(2):238–243, 2008.

[89] Ranin Atwi, Alain Tuel, Marion Maffre, Laurence Burel, Jean-Luc Rousset, and Frederic Meunier. Highly dispersed au, ag and au-ag alloy nanoparticles encapsulated in single crystal multi-hollow silicalite-1. *Applied Catalysis A: General*, 569:86–92, 2019.

[90] Mihail Mihaylov, Helmut Knoezinger, Konstantin Hadjiivanov, and Bruce C Gates.

Characterization of the oxidation states of supported gold species by ir spectroscopy of adsorbed co. *Chemie Ingenieur Technik*, 79(6):795–806, 2007.

[91] Helen Daly, Alexandre Goguet, Christopher Hardacre, FC Meunier, R Pilasombat, and D Thompsett. The effect of reaction conditions on the stability of au/cezro4 catalysts in the low-temperature water–gas shift reaction. *Journal of Catalysis*, 273(2):257–265, 2010.

[92] Flora Boccuzzi, Giuseppina Cerrato, Francesco Pinna, and Giorgio Strukul. Ftir, uv-vis, and hrtem study of au/zro2 catalyst: Reduced reactivity in the co- o2 reaction of electron-deficient gold sites present on the used samples. *The Journal of Physical Chemistry B*, 102(30):5733–5736, 1998.

[93] Alberto Villa, Nikolaos Dimitratos, Carine E Chan-Thaw, Ceri Hammond, Gabriel M Veith, Di Wang, Maela Manzoli, Laura Prati, and Graham J Hutchings. Characterisation of gold catalysts. *Chemical Society Reviews*, 45(18):4953–4994, 2016.

[94] Flora Boccuzzi, Anna Chiorino, and Maela Manzoli. Au/tio2 nanostructured catalyst: effects of gold particle sizes on co oxidation at 90 k. *Materials Science and Engineering: C*, 15(1-2):215–217, 2001.

[95] Emma K Gibson, Andrew M Beale, C Richard A Catlow, Arunabhiram Chutia, Diego Gianolio, Anna Gould, Anna Kroner, Khaled MH Mohammed, Michal Perdjon, Scott M Rogers, et al. Restructuring of aupd nanoparticles studied by a combined xafs/drifts approach. *Chemistry of Materials*, 27(10):3714–3720, 2015.

[96] Chen Zhou, Hio Tong Ngan, Jin Soo Lim, Zubin Darbari, Adrian Lewandowski, Dario J Stacchiola, Boris Kozinsky, Philippe Sautet, and Jorge Anibal Boscoboinik. Dynamical study of adsorbate-induced restructuring kinetics in bimetallic catalysts using the pdau (111) model system. *Journal of the American Chemical Society*, 144(33):15132–15142, 2022.